

SEARCH FOR THE FLAVOR-CHANGING NEUTRAL CURRENT IN TOP
PAIR EVENTS WITH AN ASSOCIATED PHOTON USING 13 TEV
PROTON-PROTON COLLISION DATA COLLECTED WITH THE ATLAS
DETECTOR

by

JASON TYLER BARKELOO

A DISSERTATION

Presented to the Department of Physics
and the Graduate School of the University of Oregon
in partial fulfillment of the requirements
for the degree of
Doctor of Philosophy

March 2020

DISSERTATION APPROVAL PAGE

Student: Jason Tyler Barkeloo

Title: Search for the Flavor-Changing Neutral Current in Top Pair Events With an Associated Photon Using 13 TeV Proton-Proton Collision Data Collected With the ATLAS Detector

This dissertation has been accepted and approved in partial fulfillment of the requirements for the Doctor of Philosophy degree in the Department of Physics by:

David Strom	Chair
James Brau	Advisor
Spencer Chang	Core Member
Dev Sinha	Institutional Representative

and

Janet Woodruff-Borden	Vice Provost and Dean of the Graduate School
-----------------------	--

Original approval signatures are on file with the University of Oregon Graduate School.

Degree awarded March 2020

© 2020 Jason Tyler Barkeloo

This work is licensed under a Creative Commons

Attribution-NonCommercial-NoDerivs (United States) License.

DISSERTATION ABSTRACT

Jason Tyler Barkeloo

Doctor of Philosophy

Department of Physics

March 2020

Title: Search for the Flavor-Changing Neutral Current in Top Pair Events With an Associated Photon Using 13 TeV Proton-Proton Collision Data Collected With the ATLAS Detector

Abstract for FCNC here.

This dissertation includes previously published and unpublished co-authored material.

CURRICULUM VITAE

NAME OF AUTHOR: Jason Tyler Barkeloo

GRADUATE AND UNDERGRADUATE SCHOOLS ATTENDED:

University of Oregon, Eugene, Oregon
Miami University, Oxford, Ohio
Wittenberg University, Springfield, Ohio

DEGREES AWARDED:

Doctor of Philosophy, Physics, 2020, University of Oregon
Master of Science, Physics, 2012, Miami University
Bachelor of Science, Physics, 2010, Wittenberg University

PROFESSIONAL EXPERIENCE:

University of Oregon, Graduate Research Assistant, ATLAS Experiment, June 2014-Present

University of Oregon, Graduate Teaching Assistant, September 2012-June 2014

Miami University, Teaching and Research Assistant, August 2010 - May 2012

Wittenberg University, Undergraduate Researcher, August 2008 - May 2010

GRANTS, AWARDS AND HONORS:

Weiser Senior Teaching Assistant Award – University of Oregon – 2014

American Association of Physics Teachers Outstanding Teaching Assistant – Miami University – 2012

PUBLICATIONS:

- A. Hachtel, J. Kleykamp, D. Kane, M. Marshall, B. Worth, J. Barkeloo, J. Kangara, J. Camenisch, M. Gillette, S. Bali. “An undergraduate lab on measurement of radiative broadening in atomic vapor”, Am. J. Phys. **81**(6), 471 (2013).

J. Kangara, A. Hachtel, M. C. Gillette, J. Barkeloo, E. Clements, S. Bali. “Design and construction of cost-effective fail-safe tapered amplifier systems for laser cooling and trapping experiments”, Am. J. Phys. **82**(8), 805 - 817 (2014).

TABLE OF CONTENTS

Chapter	Page
I. INTRODUCTION	1
1.1. The Standard Model Top Quark	1
1.2. Searching for FCNC Top Quark Decays	2
II. THEORY	4
2.1. The Standard Model Particles	4
2.2. The Standard Model Interactions	6
2.3. Electroweak Symmetry Breaking	8
2.3.1. Gauge Boson Masses	9
2.3.2. Fermion Masses	10
2.3.3. The CKM Matrix	12
2.4. The Top Quark	13
2.4.1. Discovering The Top Quark	14
2.4.2. Production and Decay At Hadron Colliders	16
2.4.3. Beyond the Standard Model Top Quark Physics	20
2.5. The Flavor-Changing Neutral Current	21
2.5.1. The Standard Model Flavor Sector	21
2.5.2. The GIM Mechanism	23
2.5.3. New Physics With Enhancements to FCNCs	26

Chapter	Page
2.5.4. Current Measurements of Top FCNCs	29
III. THE LARGE HADRON COLLIDER AND THE ATLAS DETECTOR	34
3.1. The Large Hadron Collider	34
3.1.1. LHC Magnets	37
3.1.2. Luminosity	37
3.1.3. Pileup	39
3.2. The ATLAS Detector	41
3.2.1. Coordinate System	44
3.2.2. Magnet Setup	44
3.2.3. Inner Detector	45
3.2.4. Middle Layers, EMCal, HCal	45
3.2.5. Muon Calorimeter	46
3.2.6. Trigger and Data Acquisition	47
IV. SIMULATION	49
4.1. Simulation of pp collisions	49
4.1.1. MC Generators Used for LHC Physics	49
4.1.2. Detector Simulation	49
4.1.3. Showering in the Detector	49
4.2. Object Reconstruction	49
4.2.1. Electrons	49
4.2.2. Photons	49

Chapter		Page
4.2.3.	Jets	49
4.2.4.	Muons	49
4.2.5.	Creation of FCNC Signal Events	49
V.	SEARCH STRATEGY	50
5.1.	Major Backgrounds	50
5.2.	Event Reconstruction	50
5.3.	Data and Simulation Event PreSelection	50
5.4.	Control and Validation Regions	50
5.5.	Signal Region	50
5.6.	Neural Network	50
5.6.1.	Architecture and Studies	50
VI.	RESULTS	51
6.1.	Uncertainties	51
6.2.	Statistical Treatment of Results	51
6.3.	Limit on Branching Ratio $t \rightarrow q\gamma$	51
VII.	COMPLEMENTARY SEARCHES AND OUTLOOK	52
7.1.	Comparison with Complementary Searches	52
7.2.	Future Directions	52
7.3.	Conclusion	52

Chapter	Page
REFERENCES CITED	53

LIST OF FIGURES

Figure	Page
2.1. Summary of $t\bar{t}$ production cross sections as a function of center of mass energy at Fermilab's Tevatron and CERN's LHC	15
2.2. Summary of single-top production cross sections as a function of center of mass energy at Fermilab's Tevatron and CERN's LHC.	16
2.3. Leading order diagrams for $t\bar{t}$ production at hadron colliders	17
2.4. Leading order diagrams for single top quark production	18
2.5. Top quark decays in the Standard Model	18
2.6. Categorization of top quark pair decays in the Standard Model based on the decays of the W bosons	20
2.7. Box diagram of $K_L^0 \rightarrow \mu^+\mu^-$ through the exchange of W bosons	23
2.8. Box diagrams of $K_L^0 \rightarrow \mu^+\mu^-$ through the exchange of W bosons after the inclusion of the charm quark	24
2.9. An example loop diagram of a top quark decaying to a light quark and a photon	25
2.10. Flavor-changing neutral current top quark decays.	29
2.11. Flavor-changing limits from a variety of experiments in every channel $t \rightarrow uX(\text{top})$ and $r \rightarrow cX(\text{bottom})$	30
2.12. FCNC diagram for the search in single top production at the electron-proton collider HERA.	31
2.13. FCNC diagram for the search in single top production at the electron-positron collider, LEP.	31
2.14. Flavor-changing neutral current theoretical branching ratios and experimental limits (both ATLAS and CMS) updated through 2018.	32
3.1. Map of LHC and the various detector experiments: ATLAS, CMS, LHCb, and ALICE located under the Franco-Swiss border near Geneva	35

Figure	Page
3.2. Schematic of the CERN accelerator complex.	36
3.3. Total integrated luminosity as a function of time delivered by the LHC(green), recorded (yellow) and declared good for physics analysis (blue) by the ATLAS detector throughout Run 2 consisting entirely of 13 TeV pp collisions (figure from the ATLAS Collaboration).	39
3.4. Luminosity-weighted distribution of the mean number of interactions per bunch crossing for the entirety of Run 2 shown by individual years, 2015 (yellow), 2016(orange), 2017 (purple), 2018 (green), as well as an integrated total (blue) (figure from the ATLAS Collaboration).	40
3.5. A candidate dimuon event ($Z \rightarrow \mu^+ \mu^-$) with 28 reconstructed vertices collected in 2018 with the ATLAS detector.	41
3.6. A candidate dimuon event ($Z \rightarrow \mu^+ \mu^-$) with 65 reconstructed vertices collected in 2017 with the ATLAS detector.	41
3.7. Schematic of the ATLAS detector.	42
3.8. Cross section of a simulated ATLAS detector showing how various particles interact with ATLAS subsystems.	43
3.9. Coordinate system used in the ATLAS Collaboration.	44
3.10. Schematic of the windings of the ATLAS magnet.	44
3.11. Schematic of the ATLAS inner detector.	45
3.12. Blown up schematic of the ATLAS inner detector with more detail.	45
3.13. Schematic of the ATLAS hadronic and electromagnetic calorimeter systems.	46
3.14. Schematic of the ATLAS muon detector.	47
3.15. Flow diagram of the ATLAS trigger and data acquisition system used in Run 2.	48

LIST OF TABLES

Table	Page
2.1. Particles of the Standard Model	6
2.2. Summary of the Standard Model field contents and their representations in the gauge group, labeled by their dimension ($SU(3)_C$ and $SU(2)_L$) and weak hypercharge ($U(1)_Y$)	7
2.3. Summary of final states of a W boson, when accounting for color permutations and the CKM matrix	19
2.4. Expected branching ratios for various flavor-changing neutral current processes in the Standard Model and multiple theories that predict enhancements to the branching ratio. Two-Higgs Double Models with flavor-violating Yukawa couplings (2HDM), quark single models (QS), minimal supersymmetry models with 1TeV squarks and gluinos (MSSM), R-parity violating supersymmetry models (RPV), and extra-dimensional models (XD).	26

CHAPTER I

INTRODUCTION

The Standard Model of particle physics has proven itself an exceptional and resilient theory since the combination of the electromagnetic and weak interactions in 1961[1]. Further theoretical work combined the Higgs Mechanism[2, 3] with the electroweak theory[4, 5]. The resiliency of this theoretical model has been tested to further degrees of accuracy over the decades with one of my most recent portions being the experimental confirmation of the Higgs Boson in 2012[6, 7] using the Large Hadron Collider (LHC). Further precision measurements are ongoing at various experiments at the LHC, including the ATLAS experiment.

However, the Standard Model is known to have flaws and disagreements with nature. For example, the Standard Model predicts massless neutrinos which is in conflict with experimental observation of neutrino flavor oscillation and does not provide an explanation for dark matter particles or their interactions with currently known particles. While these large gaps in the Standard Model are well known, every precision measurement made has yet to give any significant new hints toward physics beyond the Standard Model. One new pathway to look for these hints at the LHC is through top quark decays.

1.1. The Standard Model Top Quark

The top quark was first observed at Fermilab's Tevatron in 1995[8] but the increase in energy and amount of data at the LHC has produced orders of magnitude more top quarks than previously seen, opening up a pathway to precision measurements of the properties of the top quark. The top quark is the heaviest

fundamental particle with a mass of 172.51 ± 0.27 (stat) ± 0.42 (syst)[9]. This large mass also means that the top quark lifetime is very short ($5 * 10^{-25}$ s) and decays before it can hadronize. This allows the study of its branching ratios and decay modes directly. The Standard Model predicts that the top quark decays through the charged current mode nearly 100% of the time, $t \rightarrow qW$ ($q = b, s, d$)[10]. The Standard Model also predicts a rare branching ratio of the top quark through a flavor changing neutral current (FCNC) process, to a neutral boson (photon, Z boson, Higgs Boson, or gluon) and up type quark with a heavily suppressed branching ratio on the order of 10^{-14} .

1.2. Searching for FCNC Top Quark Decays

Precision measurements are an important litmus test for the Standard Model. Predicted branching ratios for FCNC processes in top quark decays are far beyond the experimental reach of the LHC and any observation of these decay modes would be a sure sign of new physics. Branching ratios are an important measurement due to a litany of theories for new physics beyond the Standard Model (BSM). These BSM theories such as Minimal Supersymmetric models[11], R-parity-violating Supersymmetric models[12] and two Higgs doublet models[13] predict enhancements in the top sector by many orders of magnitude. Even a null result of a search will set an upper limit on the branching ratio that can assist in ruling out future physical models based on their amount of large top sector enrichment.

This dissertation presents a search for top FCNCs using the entire Run 2 dataset at the LHC, containing combined 2015-2018 datasets taken by the ATLAS experiment totaling 139 fb^{-1} of integrated luminosity taken at $\sqrt{s} = 13 \text{ TeV}$. This analysis looks for an excess of events coming from top quark pair produced events where one top quark decays to the most likely decay mode (a bottom quark and W boson) and

the other to an up type quark (up or charm) and a photon. Chapter II presents a theoretical background for the Standard Model with a closer view on the usual extensions to include the FCNC vertices. Following this, Chapter III will discuss the LHC and the ATLAS experiment used in the creation of the dataset used in the analysis. In Chapter IV the special signal simulation requirements will be presented as well as the common background event simulation methodology. The search strategy including the creation of signal, control and validation regions and the training of a neural network will be examined in Chapter V. Chapter VI will discuss the results and the conclusions drawn from these results will be presented in Chapter VII.

CHAPTER II

THEORY

In this chapter a theoretical background will be presented on the Standard Model of particle physics with special attention paid to the top quark's properties and decays. This will include discussion of all of the fundamental particles and their interactions through the fundamental forces of nature: electromagnetism and the strong and weak nuclear forces.

2.1. The Standard Model Particles

The Standard Model of particle physics is the cornerstone of our understanding of the basic building blocks of nature and their interactions. Typical matter is made up of atoms consisting of electrons around an inner nucleus of protons and neutrons. These protons and neutrons are made up of a collection of up and down type quarks along with sea quarks and gluons. Protons consist of two up type quarks and a down type quark, while neutrons contain two down type quarks and a single up type quark.

Within the Standard Model all matter (quarks and leptons) is made up of fermions (spin- $\frac{1}{2}$ particles). In addition to the up and down type quarks and the electron the remaining fermions can be described as additional 'generations' that are similar, each consisting of two quarks and a lepton. Every generation consists of quarks with electric charge $+\frac{2}{3}$ and $-\frac{1}{3}$ and a lepton with charge -1 along with an electrically neutral lepton called a neutrino. All of these fermions are listed in Table 2.1.

While we can observe the leptons in nature, free quarks do not exist. We can observe quarks only as part of a bound state called a hadron. If a hadron consists of a

quark-antiquark pair ($q\bar{q}$) it is called a meson. Sets of three quarks or three antiquarks (qqq or $\bar{q}\bar{q}\bar{q}$) are called baryons. Protons and neutrons are baryonic matter.

In addition to the fermions the Standard Model contains gauge, or vector, bosons which are spin-1 particles that carry the fundamental forces of nature. The electromagnetic force is mediated by the massless, charge neutral photon (γ). The nuclear weak force is carried by two massive bosons: the electrically neutral Z boson and the charged (± 1) W boson. These bosons together dictate electroweak interactions within the Standard Model. The remaining force, the nuclear strong force, is carried through the gluon (g). Gluons are massless and chargeless but carry color, an analog of electric charge in the electroweak interaction. The last remaining piece of the Standard Model is the scalar (spin-0) Higgs boson. This Higgs boson is a massive electrically neutral boson that is responsible for giving mass to the massive fundamental particles. All of these bosons are also shown in Table 2.1.

	Particle	Spin	Charge	Mass
Quarks				
u type	u			$2.4^{+0.6}_{-0.4}$ MeV
	c	$\frac{1}{2}$	$\frac{2}{3}$	1.28 ± 0.03 GeV
	t			173.1 ± 0.6 GeV
d type	d			$4.7^{+0.5}_{-0.4}$ MeV
	s	$\frac{1}{2}$	$-\frac{1}{3}$	96^{+8}_{-4} MeV
	b			$4.18^{+0.04}_{-0.03}$ GeV
Leptons				
e doublet	e	$\frac{1}{2}$	-1	$0.5109989461 \pm 0.000000003$ MeV
	ν_e		0	< 2 eV
μ doublet	μ	$\frac{1}{2}$	-1	$105.6583745 \pm 0.0000024$ MeV
	ν_μ		0	< 2 eV
τ doublet	τ	$\frac{1}{2}$	-1	1776.86 ± 0.12 GeV
	ν_τ		0	< 2eV
Bosons				
Vector	γ	1	0	$< 10^{-18}$ eV
	g	1	0	0
	W	1	\pm	80.385 ± 0.0015 GeV
	Z	1	0	91.1876 ± 0.0021 GeV
Scalar	H	0	0	$125.09 \pm 0.21 \pm 0.11$ GeV

TABLE 2.1. Particles of the Standard Model [10]

2.2. The Standard Model Interactions

In addition to describing these particles the Standard Model also describes the ways in which these particles are capable of interacting. All of the particles described in the previous section are included in the following theory. The Standard Model Lagrangian is simply a function of fields and their derivatives taken at one point in spacetime, x^μ .

$$\mathcal{L}[\phi_i(x), \partial_\mu \phi_i(x)]$$

The Standard Model is defined having a gauge symmetry

$$G_{SM} = SU(3)_C \times SU(2)_L \times U(1)_Y$$

Name	Field Components	$(SU(3)_C, SU(2)_L, U(1)_Y)$	Comments
Spin-1/2 Quarks			
Q	$(u_L \ d_L)$ u_R d_R	$(3,2,\frac{1}{6})$ $(3,1,\frac{2}{3})$ $(3,1, -\frac{1}{3})$	x3 generations
Spin-1/2 Leptons			
L	$(\nu_L \ e_L)$ e_R	$(1,2,-\frac{1}{2})$ $(1,1,-1)$	x3 generations
Spin-0 Higgs			
ϕ	$(\phi^+ \ \phi^0)$	$(1,2,\frac{1}{2})$	
Spin-1 Gauge Bosons			
Gluons	$G^{1,...,8}$	$(8,1,0)$	
W	$(W^1 \ W^2 \ W^3)$	$(1,3,0)$	
B	B^0	$(1,1,0)$	

TABLE 2.2. Summary of the Standard Model field contents and their representations in the gauge group, labeled by their dimension ($SU(3)_C$ and $SU(2)_L$) and weak hypercharge ($U(1)_Y$)

where all of the particle content described in Section 2.1 is described under this symmetry in Table 2.2[14]. The eight color-anticolor combinations of spin-1 gluons are associated with $SU(3)_C$ where the C denotes 'color' quantum numbers of the gauge group. Any particle that carries color will interact with gluons via the strong nuclear interaction. The three spin-1 gauge bosons W_a , $a = 1, 2, 3$ conduct the weak isospin $SU(2)_L$ symmetry where the L denotes that only left-handed chiral fermions transform with respect to this symmetry. The left-handed fermions are $SU(2)$ doublets while the right-handed components are singlets. The remaining spin-1 gauge boson, B, is associated with $U(1)^Y$ weak hypercharge.

The W^\pm , Z , and photon (γ) are produced by spontaneous symmetry breaking $SU(2)_L \times U(1)_Y$ implied by the Higgs potential discussed Section 2.3.

One general way of expressing the Standard Model Lagrangian is

$$\mathcal{L}_{SM} = \mathcal{L}_{kinetic} + \mathcal{L}_{Higgs} + \mathcal{L}_{Yukawa}$$

where we have a kinetic term for the bosons and fermions, a Higgs term which includes the Higgs kinetic term and potential, and a term that dictates the Yukawa interactions. This can be expanded out

$$\mathcal{L} = \left(-\frac{1}{4} F_{\mu\nu} F^{\mu\nu} + i\bar{\psi} \not{D} \psi + \text{h.c.} \right) + (\bar{\psi}_i Y_{ij} \psi_j \phi + \text{h.c.}) + (|D_\mu \phi|^2 + V(\phi))$$

All of the gauge field strengths are included within $F_{\mu\nu}$. To maintain gauge invariance for the kinetic terms the derivative must be replaced by the covariant derivative

$$\partial^\mu \rightarrow D^\mu = \partial^\mu + ig_s G_a^\mu L_a + ig W_a^\mu T_a + ig' B^\mu Y$$

The eight gluon fields are described by G_a^μ , the three weak interaction boson fields are described by W_a^μ , and the hypercharge boson field is B^μ . Here g_s , g , and g' are the gauge coupling constants, and L_a , T_a , and Y are the generators for $SU(3)_C$, $SU(2)_L$, and $U(1)_Y$ respectively. The generators are described by the Gell-Man matrices for L_a ($\frac{1}{2}\lambda_a$ for triplets, 0 for singlets), the Pauli matrices for T_a ($\frac{1}{2}\sigma_a$ for doublets, 0 for singlets), and the $U(1)_Y$ charges for Y .

2.3. Electroweak Symmetry Breaking

The spin-1 particles within the Standard Model are massless; however we know that the real bosons made up of these states are massive (i.e. the W^\pm and Z). This comes about from a spontaneous symmetry breaking of $SU(2)_L \times U(1)_Y$ by a particle

whose ground state is not invariant under the symmetry. The scalar Higgs field is capable of doing this while at the same time not breaking the $SU(3)_C$ symmetry leaving the gluons massless because ϕ is an $SU(3)_C$ singlet.

Expanding the Yukawa term of the Lagrangian we see that the covariant derivative of the scalar field becomes

$$D_\mu \phi = \partial_\mu \phi - \frac{i}{2} (g W_\mu^a \frac{\sigma^a}{2} + g' B_\mu) \phi$$

and the potential

$$V(\phi) = \lambda (\phi^\dagger \phi - \frac{\mu^2}{2\lambda})^2 = \lambda (\phi^\dagger \phi)^2 - \mu^2 \phi^\dagger \phi + \frac{\mu^4}{4\lambda}$$

It follows that if $\frac{\mu^2}{\lambda} > 0$ then this potential has a non-zero vacuum expectation value $v^2 \equiv \frac{\mu^2}{\lambda}$. The condition $\lambda > 0$ is a requirement on the vacuum stability of the model such that $\mu^2 < 0$ is the requirement for spontaneous symmetry breaking. Therefore we can make a gauge transformation such that

$$\langle \phi \rangle = \frac{1}{\sqrt{2}} \begin{pmatrix} 0 \\ v \end{pmatrix}$$

2.3.1. Gauge Boson Masses

The mass eigenstates of the spin-1 bosons can be recovered from this by writing out the mass part of the gauge boson kinetic term $|D^\mu \phi|^2$

$$\mathcal{L}_{mass} = -\frac{1}{8} \begin{pmatrix} 0 & v \end{pmatrix} \begin{pmatrix} gW_3 + g'B & g(W_1 - iW_2) \\ g(W_1 + iW_2) & -gW_3 + g'B \end{pmatrix}^2 \begin{pmatrix} 0 \\ v \end{pmatrix}$$

and if we define the weak mixing angle as $\tan\theta_W \equiv \frac{g'}{g}$ and the mass eigenstates of the bosons

$$W^\pm \equiv \frac{1}{\sqrt{2}}(W_1 \mp iW_2)$$

$$Z \equiv \cos\theta_W W_3 - \sin\theta_W B$$

$$A \equiv \sin\theta_W W_3 + \cos\theta_W B$$

then the mass matrix can be diagonalized to give

$$\mathcal{L}_{mass} = -\frac{1}{4}g^2 v^2 W^+ W^- - \frac{1}{8}(g^2 + g'^2)v^2 Z^2$$

which gives us the masses of our bosons: $M_W^2 = \frac{1}{4}g^2 v^2$, $M_Z^2 = \frac{1}{4}(g^2 + g'^2)v^2$, and $M_A^2 = 0$. Since the field A is massless there is an unbroken $U(1)$ that is identified as the photon and $U(1)_{EM}$.

2.3.2. Fermion Masses

Fermions acquire their masses from the Yukawa term in the Lagrangian. If we transform into the mass basis, also using the replacement of the scalar field corresponding to a physical Higgs boson

$$\phi = \frac{1}{\sqrt{2}} \begin{pmatrix} 0 \\ v + H(x) \end{pmatrix}$$

then we can write the $SU(2)_L$ quark doublets into their components

$$Q_{Li} = \begin{pmatrix} U_{Li} \\ D_{Li} \end{pmatrix}$$

The Yukawa term can be broken down into a baryonic and leptonic portion. The lepton portion leads to charged lepton masses after the Higgs acquires a vacuum expectation value after electroweak symmetry breaking.

$$-\mathcal{L}_{\text{Yukawa}}^{\text{leptons}} = Y_{ij}^e \overline{L}_{Li} \phi E_{Rj}$$

This leads to three physical parameters, which are generally chosen to be the three charged lepton masses (electron, muon, tau). The baryonic term leads to quark masses and flavors. Ten physical parameters arise from the baryonic Yukawa interactions

$$-\mathcal{L}_{\text{Yukawa}}^{\text{quarks}} = Y_{ij}^d \overline{Q}_{Li} \phi D_{Rj} + Y_{ij}^u \overline{Q}_{Li} \tilde{\phi} U_{Rj} + \text{h.c.}$$

Expanding this in terms of the above $SU(2)_L$ components

$$-\mathcal{L} = (M_d)_{ij} \overline{D}_{Li} D_{Rj} + (M_u)_{ij} \overline{U}_{Li} U_{Rj} + \text{h.c.}$$

such that $M_q = \frac{v}{\sqrt{2}} Y^q$. Unitary matricesies (V_{qL} and V_{qR}) that take us to the mass basis can always be found.

$$V_{qL} M_q V_{qR}^\dagger = M_q^{\text{diag}}, \text{ for } q=u,d$$

The quark mass eigenstates that follow from this are:

$$q_{Li} = (V_{qL})_{ij} q_{Lj}^I \text{ and } q_{Ri} = (V_{qR})_{ij} q_{Rj}^I$$

being transformed from the interaction basis I .

2.3.3. The CKM Matrix

In the interaction basis interactions between quarks and W^\pm come from the $\psi \not{D} \psi$ kinetic term in the Lagrangian. We can explicitly write this out in both the interaction and mass basis such that:

$$\text{Interaction Basis: } -\mathcal{L}_{W^\pm}^q = \frac{g}{2} \overline{Q}_{Li} \gamma^\mu W_\mu^a \tau^a Q_{Li} + \text{h.c.}$$

$$\text{Mass Basis: } -\mathcal{L}_{W^\pm}^q = \frac{g}{\sqrt{2}} \begin{pmatrix} \bar{u}_L & \bar{c}_L & \bar{t}_L \end{pmatrix} \gamma^\mu (V_{uL} V_{dL}^\dagger)_{ij} W_\mu^+ \begin{pmatrix} d_L \\ s_L \\ b_L \end{pmatrix} + \text{h.c.}$$

The term $V = V_{uL} V_{dL}^\dagger$ in the previous equation is a unitary 3×3 matrix known as the Cabibbo-Kobayashi-Maskawa (CKM) matrix [15, 16] that describes quark mixing.

The CKM matrix can be expressed simply:

$$V_{CKM} = \begin{bmatrix} V_{ud} & V_{us} & V_{ub} \\ V_{cd} & V_{cs} & V_{cb} \\ V_{td} & V_{ts} & V_{tb} \end{bmatrix}$$

The components of the CKM matrix are not all arbitrary. This can be expressed in the Wolfenstein parametrization[17] to show that there are only four parameters, three real and one complex. The Wolfenstein parameterization is an expansion in $V_{us} = \lambda \approx 0.2243$.

$$V_{CKM}^{\text{Wolfenstein}} = \begin{bmatrix} 1 - \frac{1}{2}\lambda^2 & \lambda & A\lambda^3(\rho - i\eta) \\ -\lambda & 1 - \frac{1}{2}\lambda^2 & A\lambda^2 \\ A\lambda^3(1 - \rho - i\eta) & -A\lambda^2 & 1 \end{bmatrix}$$

This formulation demonstrates quite clearly that the CKM matrix is almost diagonal but has small off-diagonal terms. This means that interactions between quarks is strongest within a generation i.e. up and down quarks, charm and strange quarks, and top and bottom quarks experience the largest degree of mixing between each other. A top quark directly decays to a bottom quark and W boson almost all of the time ($\approx 99.83\%$ of the time). While the mixing does not prohibit decaying to a strange or down quark instead of a bottom, it is a significantly rarer event ($\approx 0.16\%$ and $\approx 0.01\%$, respectively). The values for all of these parameters have been measured experimentally and are collected by the Particle Data Group[10]:

$$V_{CKM} = \begin{bmatrix} 0.97420 \pm 0.00021 & 0.2243 \pm 0.0005 & 0.00394 \pm 0.00036 \\ 0.218 \pm 0.004 & 0.997 \pm 0.017 & 0.0422 \pm 0.0008 \\ 0.0081 \pm 0.0005 & 0.0394 \pm 0.0023 & 1.019 \pm 0.025 \end{bmatrix}$$

2.4. The Top Quark

This dissertation will pay particular interest to the top quark, the heaviest of all of the fundamental particles, over 40 times heavier than its generational partner the bottom quark and 40% larger than the Higgs boson the next heaviest particle. One of its most interesting properties, due to its large mass, is that it has an extremely small lifetime ($\approx 5 \times 10^{-25}s$). This lifetime is orders of magnitude shorter than the characteristic time over which the strong nuclear interaction takes place ($\approx 10^{-23}s$), meaning that it decays before it can hadronize by combining with another quark to form a mesonic or baryonic system. This allows us to observe the decays of the top quark directly as opposed to the decay products of a top quark system. The top quark was first proposed as an explanation of CP violation in kaon decays by

Kobayashi and Maskawa in 1973[16] which predicted a third generation of quarks. At the time there was little evidence for this but the later discovery of the charm quark that was predicted to exist due to a suppression caused by the GIM mechanism[18], which formed the foundation upon which much of Kobayashi and Maskawa's work was built. The discovery of the charm filled out a complete 2 generation Standard Model (up, down, strange, and charm quarks and the electron and muon). However the further observation of the tau lepton meant that the required symmetry within the GIM mechanism would be broken without the existence of a third generation of quarks, the top and bottom. Within just a few years, in 1977, the bottom was also discovered[19] and the theoretical predictions of the Standard Model at the time heavily favored the existence of a 6th quark, the 3rd and heaviest up-type quark.

2.4.1. Discovering The Top Quark

Almost 20 years went by after the discovery of the bottom quark and many experiments came up empty handed even while discovering the W and Z bosons (the Super Proton Synchrotron at CERN) before direct evidence for the top quark was observed at Fermilab's Tevatron in both the CDF and D0 experiments in 1995[8, 20]. While the Tevatron only operated at a maximum energy of 1.96 TeV during its lifetime, further properties of the top quark could not be probed in detail due to a lack of statistics. Not until the LHC began operation at a center of mass energy of 7 TeV in 2010 were enough top quarks produced to study the details of its interactions.

The amount of top quarks produced scale up by the energy as seen in Figure 2.1 as well as the integrated luminosity, or number of events produced, of the accelerator and detector setup. The LHC has significantly more of both than the Tevatron did.

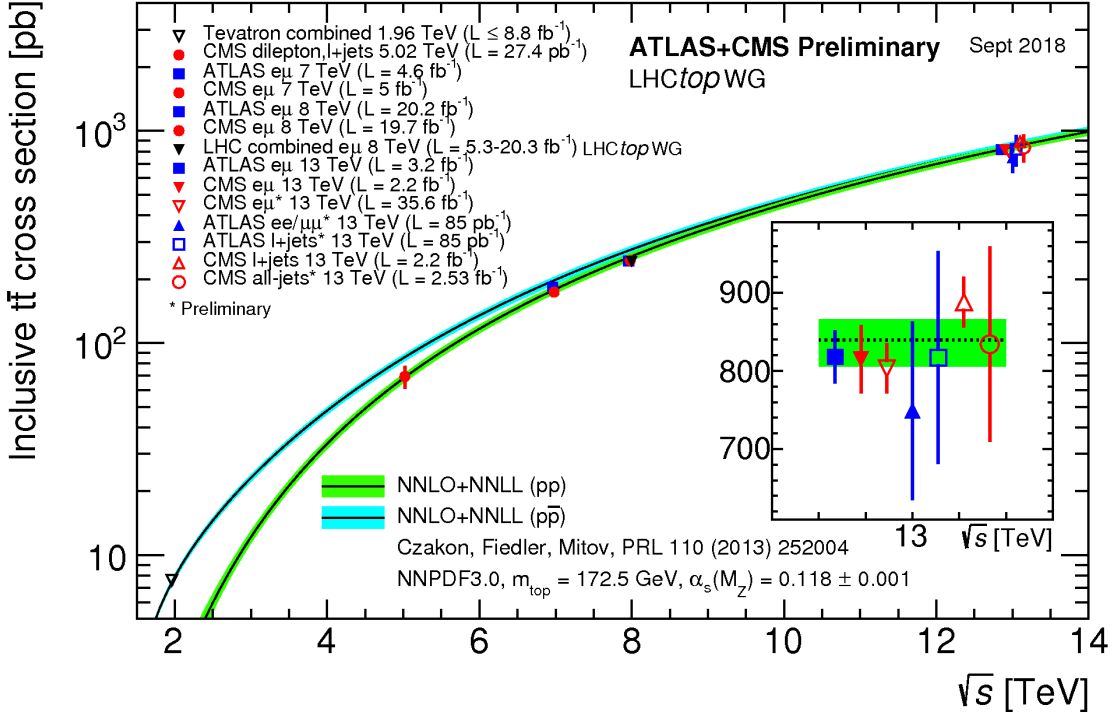


FIGURE 2.1. Summary of $t\bar{t}$ production cross sections as a function of center of mass energy at Fermilab’s Tevatron and CERN’s LHC. For a top mass of 172.5 GeV and center of mass energy of 13 TeV the central value cross section is calculated to be 831 pb

Throughout the entirety of Run 2 at the LHC there are expected to be more than 115,000 top pair events produced within the ATLAS detector., allowing physicist to probe the details of the top quark better than ever before.

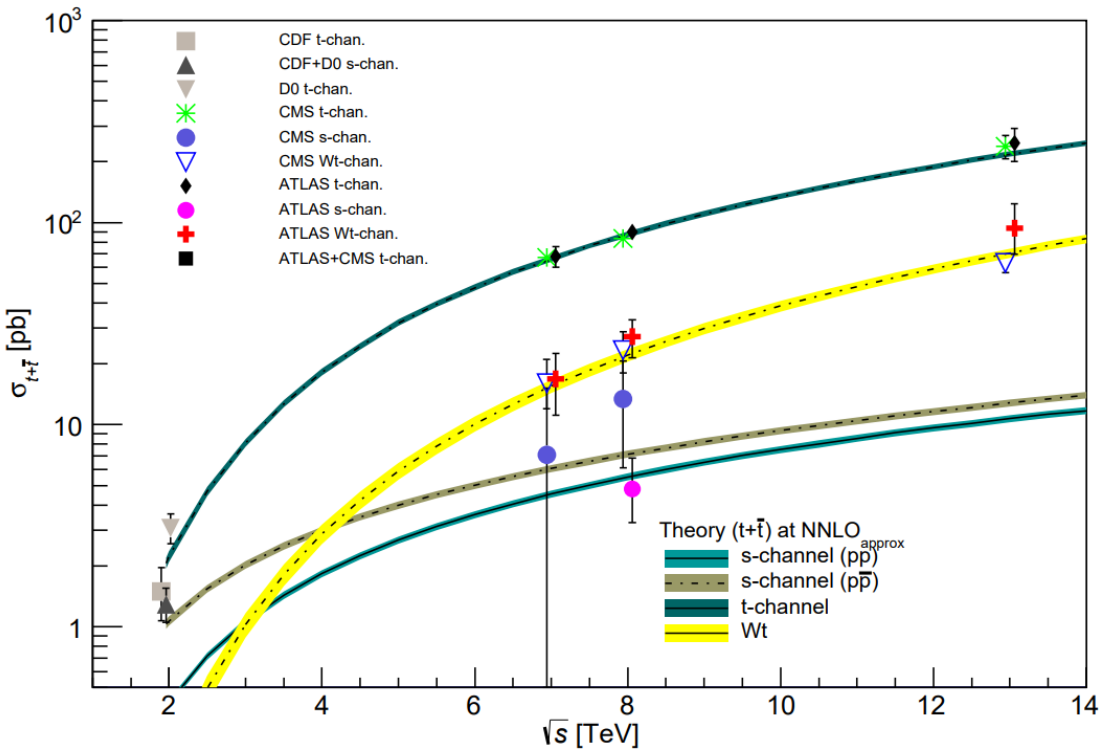


FIGURE 2.2. Summary of single-top production cross sections as a function of center of mass energy at Fermilab’s Tevatron and CERN’s LHC.

2.4.2. Production and Decay At Hadron Colliders

There are multiple ways to produce top quarks at the LHC. The most prevalent production mechanism of top quarks is through producing top/anti-top quark pairs. This can be done, to leading order, either by quark-antiquark annihilation (Figure 2.3a) or gluon gluon fusion (Figure 2.3b-d). At the Tevatron, a proton anti-proton collider, the leading diagram was quark-antiquark annihilation because of the significantly larger amount of antiquarks in the collisions. At the LHC the major production mechanism is gluon-gluon fusion, $\approx 90\%$, while quark-antiquark annihilation accounts for only $\approx 10\%$ of top quark pair production. This is a strong interaction process and is therefore quite common. The cross sections are shown in Figure 2.1.

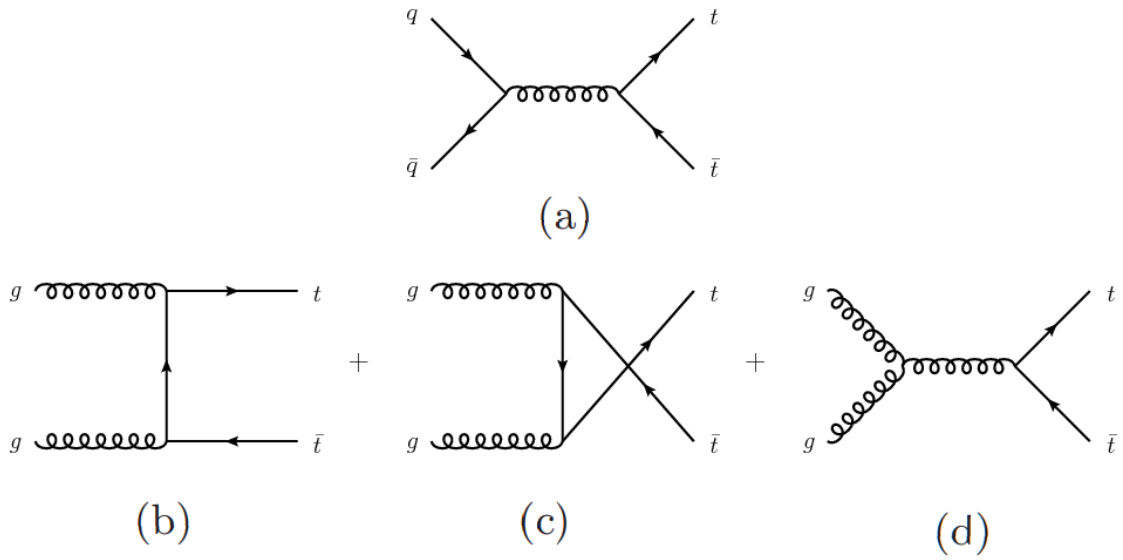


FIGURE 2.3. Leading order diagrams for the production of top/anti-top quark pairs at hadron colliders. Quark-antiquark annihilation diagram in (a) while (b)-(d) show various gluon-gluon fusion diagrams

Single top quarks can also be produced through weak interactions, which is less common, and the leading diagrams are shown in Figure 2.4 and their cross sections as measured at the LHC and Tevatron are shown in Figure 2.2. Comparing the leading production mechanisms at 13 TeV, it can be seen that $t\bar{t}$ production is about a factor of 4 larger than single top production. This means there are about 8x as many top quarks looking at pair produced events, as two are produced per event while giving an additional experimental handle in looking for an invariant mass of final state products around the top quark mass.

Because the top quark decays before hadronization, we can study the branching ratios to various products directly. Figure 2.5 shows ways the top quark is allowed to decay in the Standard Model. Figure 2.5a shows the most likely decays where the top quark decays to a down-type quark and a W boson. The branching ratio of these decays is proportional to the square of the corresponding matrix element in the CKM

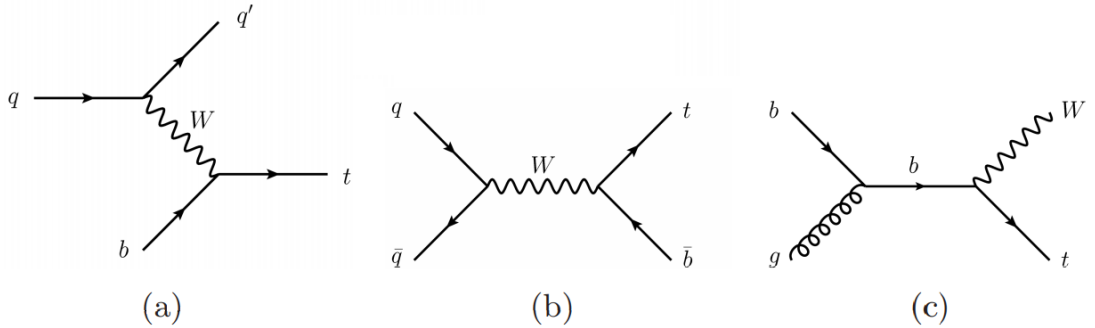


FIGURE 2.4. Leading order diagrams for the production of single top quarks at hadron colliders. The t-channel diagram is shown in (a), the s-channel in (b), and production in association with a W-boson is shown in (c)

matrix as shown in Section 2.3.3. The sum of these branching ratios is unity within standard error bars such that the implication of the diagrams, corresponding to the flavor-changing neutral current decays, shown in Figure 2.5b, are highly suppressed which will be explored further in Section 2.5.

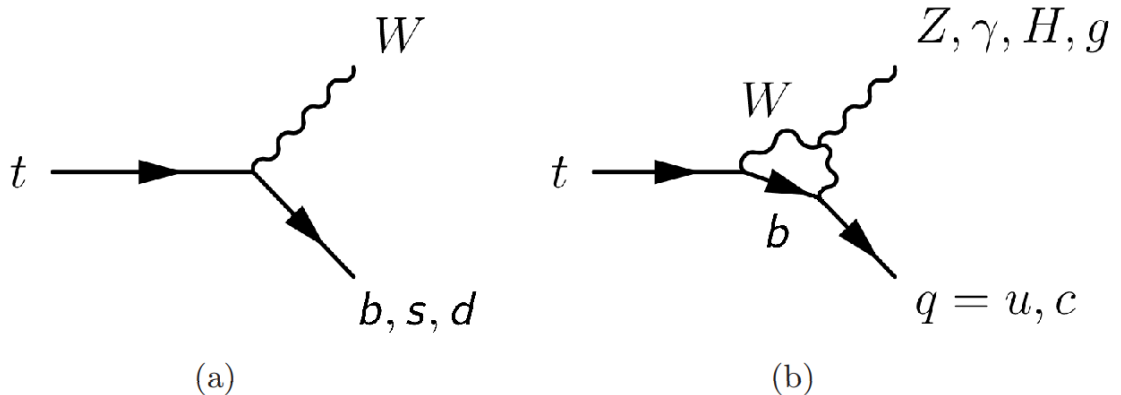


FIGURE 2.5. Top quark decays in the Standard Model

Since the matrix element V_{tb} in the CKM matrix is essentially unity each top usually decays to a b quark and a W boson. The final state of the top pair events are then typically categorized by the decay of the W bosons. The W boson can decay leptonically to a lepton (electron, muon, or tau) and its associated neutrino

Decay Mode	States	Decay Mode	States	Decay Mode	States
$W^+ \rightarrow e^+ \nu_e$	1	$W^+ \rightarrow u\bar{d}$	$\times 3 V_{ud} ^2$	$W^+ \rightarrow c\bar{d}$	$\times 3 V_{cd} ^2$
$W^+ \rightarrow \mu^+ \nu_\mu$	1	$W^+ \rightarrow u\bar{s}$	$\times 3 V_{us} ^2$	$W^+ \rightarrow c\bar{s}$	$\times 3 V_{cs} ^2$
$W^+ \rightarrow \tau^+ \nu_\tau$	1	$W^+ \rightarrow u\bar{b}$	$\times 3 V_{ub} ^2$	$W^+ \rightarrow c\bar{b}$	$\times 3 V_{cb} ^2$

TABLE 2.3. Summary of final states of a W^+ boson, when accounting for color permutations and the CKM matrix. The table holds true if you flip all particles to their antiparticles

or hadronically to quarks. This means top pair events are described as "all-hadronic" where both W bosons decay hadronically, "leptonic" if both W bosons decay leptonically, or "semi-leptonic" if one W boson decays hadronically and the other leptonically. The ratios of these events is shown in Figure 2.6. However, because of how the tau decays and interacts, these events are typically treated separately. Only the electron and muons are considered as the leptons in the "semi-leptonic" final state of a $t\bar{t}$ event. A quick counting (neglecting final state particle masses) of the final states of W bosons is shown in Table 2.3. The unitarity condition of the CKM matrix implies that $|V_{ud}|^2 + |V_{us}|^2 + |V_{ub}|^2 = 1$. The phase space of the final product then has 1 state for each of the leptons and approximately 3 for each of the up type quarks so a single top quark can be expected to decay into a lepton $\approx \frac{3}{9}$ of the time or any combination of quarks the other $\approx \frac{6}{9}$ of the time. This holds when looking at the branching ratios of top quark pairs in Figure 2.6. The end result of this is that the regions of special interest for this dissertation, the electron and muon semi-leptonic final states, occur $\approx 30\%$ of the time. While this is not the largest selection of the final state branching ratios the presence of a lepton makes it easier to look for these final states.

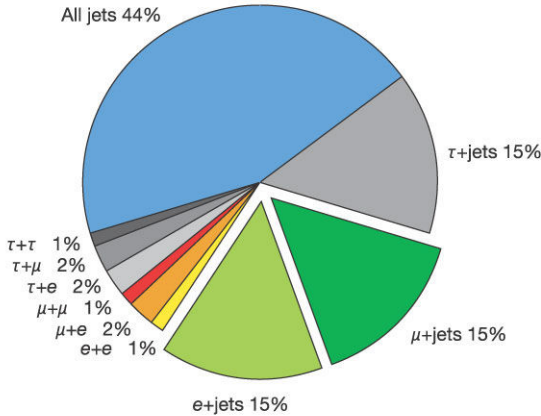


FIGURE 2.6. Categorization of top quark pair decays in the Standard Model based on the decays of the W bosons

2.4.3. Beyond the Standard Model Top Quark Physics

Many questions remain open with the intricacies of the Standard Model involving top quarks. The mass of the top quark is at a mass scale similar to the W, Z, and Higgs bosons. Does this imply the top plays a special role in the mechanism of electroweak symmetry breaking? After the discovery of the Higgs: why do the top quark and Higgs boson have the exact masses they do which allows the electroweak potential to be stable up to very high energy scales as well as allowing the Universe to sit in a meta-stable state[21]. Because of its large mass the top quark is the main destabilizer of the Higgs potential. It may be possible that new physics models will predict phenomena that can be more easily found in the properties of the top quark due to changes in the Higgs sector. Many new physics models will present most dramatically in top quarks as radiative corrections to new massive particles will effect tops first before presenting in deviations in properties of the other, significantly lighter, fermions. For example, a new Higgs like particle would most likely couple most strongly to the top quark. Now that an unprecedented number of top quarks

events are accessible, the predictions of the Standard Model can be tested with much greater precision. Top quark production modes, decay modes, couplings, and various other properties are now being measured and providing limits on the phase spaces of any new physical models that exist or ruling out entire classes of models that have yet to be written down. Arguably the properties of top quark are one of the most likely places that will point to a new understanding of our Universe.

2.5. The Flavor-Changing Neutral Current

The idea of "flavor" in the Standard Model refers to copies of the $SU(3)_C \times U(1)_{EM}$ representation, shown previously in Table 2.2. Specifically it will be used in the discussion of the generational change of one quark into another through some interaction. As an example, Figure 2.5b shows a flavor-changing neutral current interaction.

2.5.1. The Standard Model Flavor Sector

Quarks that interact with W^\pm bosons have interactions that stem from the kinetic term of the Standard Model Lagrangian. If this is written out explicitly in the mass eigenstates the interaction looks like:

$$-\frac{g}{\sqrt{2}} \begin{pmatrix} \bar{u}_L & \bar{c}_L & \bar{t}_L \end{pmatrix} \gamma^\mu W_\mu^+ V \begin{pmatrix} d_L \\ s_L \\ b_L \end{pmatrix} + \text{h.c.}$$

where the W interacts directly to change the flavor of quarks from an down(up)-type to an up(down)-type quark. The CKM matrix can be thought of as a rotation between the mass and interaction basis and the fact that the CKM matrix is non-

diagonal means that the W boson interacts with quarks of different flavors. The small off-diagonal elements of the CKM matrix mean that this generational change is a significantly smaller effect than interactions that change flavors within a generation, i.e. a top quark going to a bottom quark and W boson is much more likely than a top quark decaying to a down or strange quark and a W boson. Going two generations away from the diagonal the mixing from the CKM matrix is even smaller. The interaction with a W boson between two quarks is the only interaction vertex in the Standard Model that allows for both flavor and generation changes.

As opposed to this flavor changing charged current interaction the FCNC is an interaction between neutral gauge bosons and fermions. These FCNC processes involve either up or down type quarks or involve charged or neutral leptons. The flavor of the fermion is changed but the electric charge is conserved because it interacts with a neutral boson as opposed to the W^\pm like in the charged current interaction. FCNC interactions are forbidden at tree-level in the Standard Model but can occur via higher order processes such as loops (as shown in Figure 2.5b).

There are four neutral bosons in the Standard Model: the gluon, photon, Higgs boson, and Z boson. Each of these can mediate FCNC interactions but all are forbidden at tree-level. The gluon and photon correspond to exact gauge symmetries and have diagonal, flavor universal couplings since their interactions with fermions come through the kinetic terms. The ramification of this is that they only interact with fermions of the same flavor. The Standard Model Higgs cannot couple to fermions of different flavor since the Standard Model fermions are chiral and the Higgs couplings to fermions align with the fermion mass matrix. In the Standard Model there is only a single Higgs doublet and the only source of the fermionic masses is the Higgs vacuum expectation value. The Z boson can only connect to quarks from the

same type (up or down). When you move from the interaction to the mass eigenstates the rotation matrices only include terms such as $U_{uL}U_{uL}^\dagger = 1$ as opposed to the CKM matrix terms ($U_{uL}U_{dL}^\dagger$) which means these couplings are also flavor universal. The Standard Model FCNC suppression is built in through these means as opposed to generation-changing charged current processes. The charged current processes rely on the CKM parameters which are free parameters of the Standard Model and as such are measured and "put in." These FCNCs are suppressed multiple ways in the Standard Model.

2.5.2. The GIM Mechanism

Historically the original Cabibbo model of particle physics only had three quarks: the up, down, and strange. Studies of Kaon decay during the late 1960's suggested there were no neutral current interactions in the Standard Model at the time. The decay $K^+ \rightarrow \mu^+\nu_\mu$ was observed but the process $K_L^0 \rightarrow \mu^+\mu^-$ which was predicted was not observed. Even in the absence of a tree level decay the K_L^0 decay was still predicted via a box diagram through the exchange of W bosons shown in Figure 2.7.

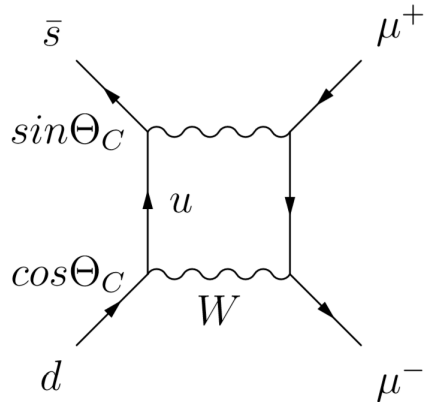


FIGURE 2.7. Box diagram of $K_L^0 \rightarrow \mu^+\mu^-$ through the exchange of W bosons

Interactions at the time were thought to have strangeness quantum number interactions that changed strangeness in the following way:

$$\Delta S = 0 : u\bar{u} + d\bar{d}\cos^2\Theta_C + s\bar{s}\sin^2\Theta_C$$

$$\Delta S = 1 : (s\bar{d} + d\bar{s})\sin\Theta_C\cos\Theta_C$$

The non-observation of the predicted decay led Glashow, Iliopoulos, and Maiani to predict the existence of a fourth quark, the charm, in 1970[18]. The addition of the charm led to two quark doublets and an almost perfect cancellation between the box diagrams:

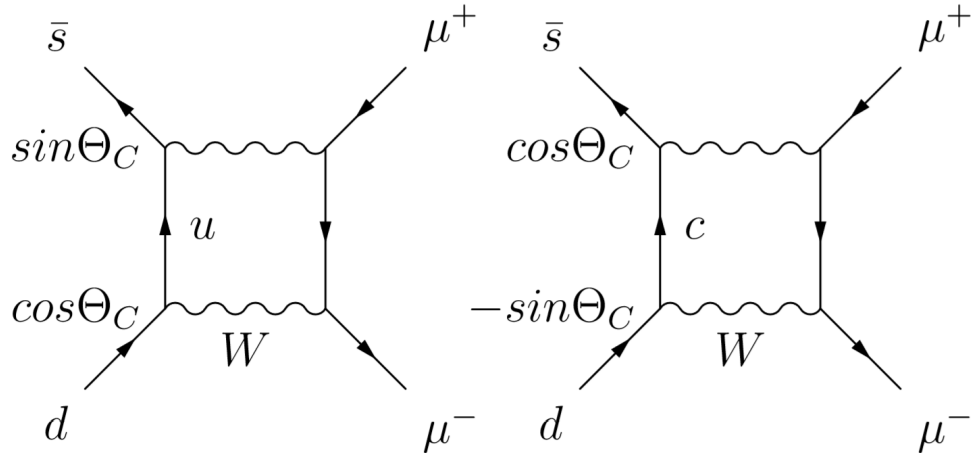


FIGURE 2.8. Box diagrams of $K_L^0 \rightarrow \mu^+\mu^-$ through the exchange of W bosons after the inclusion of the charm quark

These box diagrams mean that the strangeness change in interactions can be rewritten as

$$\Delta S = 0 : u\bar{u} + c\bar{c} + (d\bar{d} + s\bar{s})\cos^2\Theta_C + (s\bar{s} + d\bar{d})\sin^2\Theta_C$$

$$\Delta S = 1 : (s\bar{d} + d\bar{s} - d\bar{s} - s\bar{d})\sin\Theta_C\cos\Theta_C$$

The addition of the charm means that, in the approximation $m_c = m_u$, the $\Delta S = 1$ terms cancel exactly, as the new box diagrams show in Figure 2.8. The FCNC interactions in top quark decays are suppressed through this mechanism as well, with the further inclusion of the bottom and top quarks. They are further suppressed by being proportional to the quark mixing of off-diagonal elements in the CKM matrix, which are significantly less than 1. A loop diagram for top quark FCNC is shown in Figure 2.9. This loop process is very rare. The Standard Model branching ratio for these top FCNC interactions are shown along predicted enhancements from a variety of models of physics beyond the Standard Model in Table 2.4.

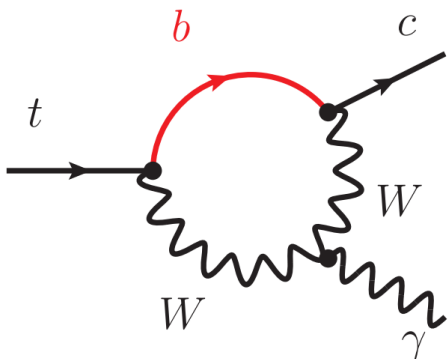


FIGURE 2.9. An example loop diagram of a top quark decaying to a light quark and a photon

Process	SM	2HDM	QS	MSSM	RPV	XD
$t \rightarrow u\gamma$	$4 * 10^{-16}$	—	$\leq 4 * 10^{-8}$	$\leq 10^{-8}$	$\leq 10^{-9}$	—
$t \rightarrow c\gamma$	$5 * 10^{-14}$	$\leq 10^{-7}$	$\leq 4 * 10^{-8}$	$\leq 10^{-8}$	$\leq 10^{-9}$	$\leq 10^{-9}$
$t \rightarrow uZ$	$7 * 10^{-17}$	—	$\leq 6 * 10^{-4}$	$\leq 10^{-7}$	$\leq 10^{-6}$	—
$t \rightarrow cZ$	$1 * 10^{-14}$	$\leq 10^{-6}$	$\leq 6 * 10^{-4}$	$\leq 10^{-7}$	$\leq 10^{-6}$	$\leq 10^{-5}$
$t \rightarrow ug$	$4 * 10^{-14}$	—	$\leq 9 * 10^{-7}$	$\leq 10^{-7}$	$\leq 10^{-6}$	—
$t \rightarrow cg$	$5 * 10^{-12}$	$\leq 10^{-4}$	$\leq 9 * 10^{-7}$	$\leq 10^{-7}$	$\leq 10^{-6}$	$\leq 10^{-10}$
$t \rightarrow uH$	$2 * 10^{-17}$	$\leq 6 * 10^{-6}$	—	$\leq 10^{-5}$	$\leq 10^{-9}$	—
$t \rightarrow cH$	$3 * 10^{-15}$	$\leq 2 * 10^{-3}$	—	$\leq 10^{-5}$	$\leq 10^{-9}$	$\leq 10^{-4}$

TABLE 2.4. Expected branching ratios for various flavor-changing neutral current processes in the Standard Model and multiple theories that predict enhancements to the branching ratio. Two-Higgs Double Models with flavor-violating Yukawa couplings (2HDM) [22, 23], quark single models (QS) [24, 25], minimal supersymmetry models with 1TeV squarks and gluinos (MSSM) [11], R-parity violating supersymmetry models (RPV) [26], and extra-dimensional models (XD) [27].

2.5.3. New Physics With Enhancements to FCNCs

Various theoretical models that include physics beyond what is included in the Standard Model are proposed to solve problems that exist with the Standard Model or an explanation of known phenomena that are not in agreement with the Standard Model. Various models seek to solve different problems, e.g., providing a dark matter candidate or fixing the naturalness problem of the Standard Model resulting from an unexpectedly high amount of fine-tuning from loop corrections to the Higgs mass. Top quark FCNCs in the Standard Model are currently so far from experimental reach (≈ 10 orders of magnitude) that they are impossible to observe even with major improvements to the accelerator and detector technologies. Table 2.4 also shows a variety of theories beyond the Standard Model which predict large enhancements to FCNC top couplings. For the most part these enhancements come from terms that have very heavy particles moving in the loops. Therefore searching for FCNCs

with top quarks provides a particularly good handle to study models of new physics and rule out the phase spaces of these models by lowering the expected limit. An explanation of the various models explored in Table 2.4 follows.

Two-Higgs-Doublet Models (2HDM): 2HDM are a simple extension of the Standard Model which contain two Higgs doublets instead of the one currently contained in the Standard Model. This leads to a much richer phenomenology in the Higgs sector with two CP even neutral Higgs bosons (h and a heavier H), a CP odd pseudoscalar A , and two charged Higgs bosons H^\pm . The currently discovered Higgs boson can be mapped to either h or H depending on various limits in the model of choice. These models can typically be described by an additional six parameters: the four Higgs masses (m_h, m_H, m_A, m_{H^\pm}), the ratio of the two vacuum expectation values and a mixing angle that diagonalizes the mass matrix of the neutral CP even Higgs bosons. Many supersymmetric models predict the existence of an extra Higgs doublet. Some of these models also attempt to explain the baryon asymmetry of the Universe[28]. 2HDM Models predict very large enhancements to FCNC interactions due to an extension of the electroweak symmetry breaking sectors. Some of these models (type III 2HDM, and models of minimal flavor violation) include tree level FCNCs[29] which is why the enhancement brings the branching ratio up to an observable level.

Quark Singlet Models (QS): QS involve an extension to the Standard Model in the form of an extra vector-like quark singlet that couples strongly to the top quark, typically in the form of a top-partner quark. These heavier t' quarks could explain the fine-tuning of the Higgs boson mass through cancellation of some or all of the top loop diagrams present in the radiative corrections to the Higgs mass. These models

generally imply then that the CKM matrix is no longer unitary and tree level FCNCs are allowed which offers a great enhancement to potential branching ratios[24, 25].

Minimal Supersymmetric Models (MSSM): Supersymmetric models where every Standard Model particle has a super particle partner typically aim to solve multiple problems with the Standard Model at once. Generally, the fact that the lightest supersymmetric particle, which is stable, provides a good dark matter candidate. MSSM models have super partner quarks (squarks) and super partner gluons (gluinos) on a mass scale of ≈ 1 TeV. Top FCNCs can occur through loop diagrams still, as they do in the Standard Model, but the loop is enhanced as it includes the supersymmetric particle of the top quark (the heavier stop quark)[11, 30].

R-Parity Violating Supersymmetric Models (RPV): Another supersymmetric model where R parity ($P_R = (-1)^{3B+L+2s}$), where B is baryon number, L is lepton number, and s is spin is no longer conserved. FCNCs can also occur at the one loop level in these models in loops which no longer conserve baryon or lepton number.[26]

Extra-dimensional Models (XD): XD Models are Randall-Sundrum models that describe the Universe as a warped-geometry higher dimensional space where elementary particles are localized on a (3+1)-dimensional brane. These models offer a potential solution to the hierarchy problem of the Standard Model by adding in a mechanism to explain the difference between the typical scales over which FCNCs take place (the electroweak scale) and the Planck scale. In these models FCNCs exist due to flavor-violating couplings between Standard Model fermions and Kaluza-Klein excitations of the gauge bosons in the Standard Model[27]. Due to their overlap with Kaluza-Klein guage modes the flavor-violating couplings will be largest in the top sector.

2.5.4. Current Measurements of Top FCNCs

All four of the neutral boson mediated FCNC channels can be searched for individually and model independently. Each channel will have its own signature and various advantages and disadvantages in performing the search. Each of the potential tree-level diagrams is shown in Figure 2.10, all of which are forbidden in the Standard Model.

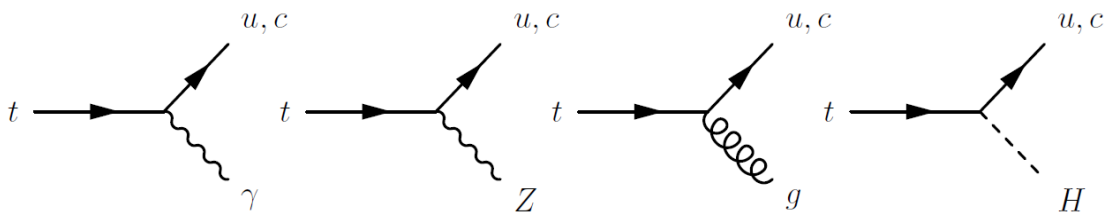


FIGURE 2.10. Flavor-changing neutral current top quark decays.

The FCNC channels involving all of the various neutral bosons can be searched for with the ATLAS detector in both single-top production modes as well as the decay mode through $t\bar{t}$ events. All of the production channels provide a sharp separation between $u \rightarrow tX$ and $c \rightarrow tX$ but have fewer statistics than decays in the decay mode using $t\bar{t}$ events. Some final states of these various FCNC events such as those involving the decay mode search for $t \rightarrow qZ$ exploit the tri-lepton final state ($Z \rightarrow ll$, with the other top decaying leptonically $t \rightarrow bW \rightarrow bl\nu$). The FCNC process involving the Higgs boson has the advantage of being able to look in a wide range of potential final states of the Higgs and can be successfully tackled using a variety of different methods.

Limits have been set on these FCNC processes at various experiments in the past. The electron-proton collider HERA at DESY, the electron-proton collider LEP at CERN, and the proton-proton colliders the Tevatron at Fermilab and the LHC at

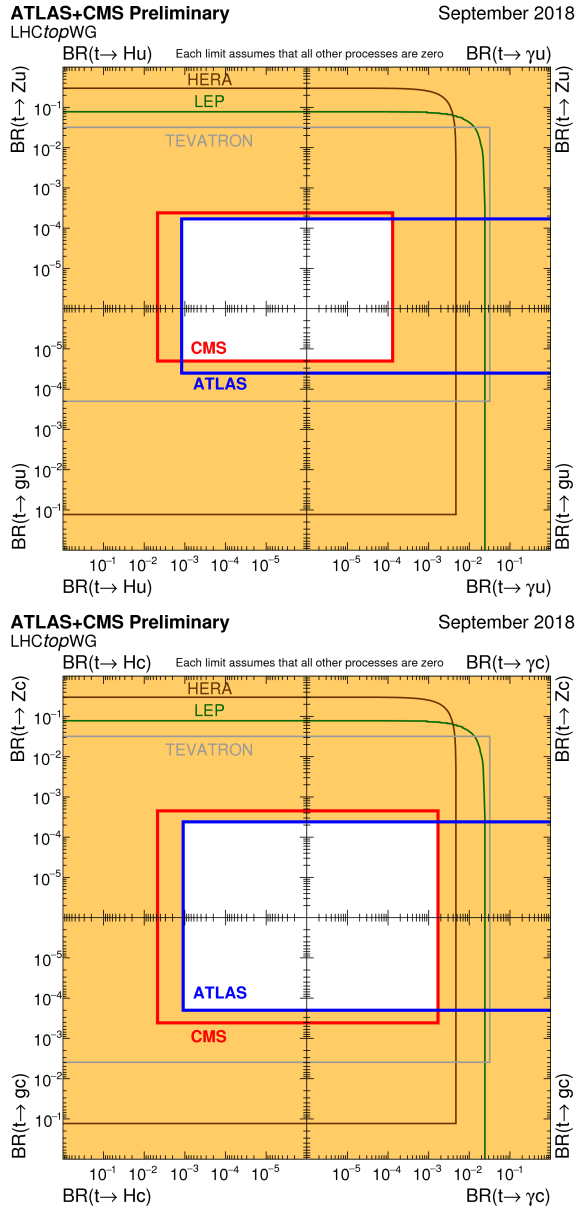


FIGURE 2.11. Flavor-changing limits from a variety of experiments in every channel $t \rightarrow uX$ (top) and $r \rightarrow cX$ (bottom)

CERN have all had experiments searching for the FCNC processes. The collected limits of these experiments are shown in Figure 2.11. Due to the energy of these early colliders 209 GeV center of mass energy for LEP and 318 GeV for HERA only production modes could be searched for as they are below the production threshold

for $t\bar{t}$ pairs. The diagrams searched for at these experiments are shown in Figure 2.12 (HERA) and Figure 2.13 (LEP).

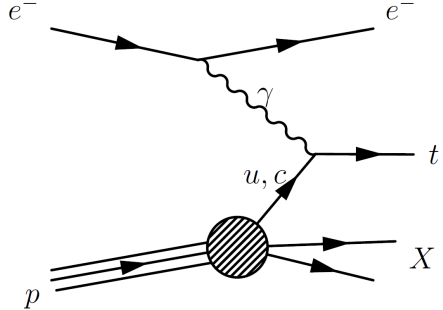


FIGURE 2.12. FCNC diagram for the search in single top production at the electron-proton collider HERA.

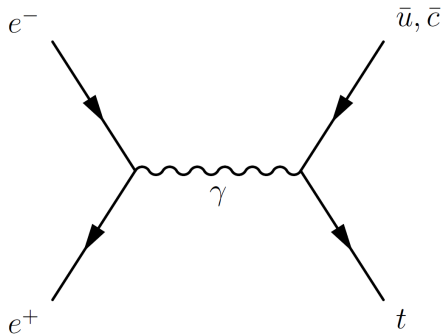


FIGURE 2.13. FCNC diagram for the search in single top production at the electron-positron collider, LEP.

Shown in Figure 2.14 are the Standard Model theoretical predictions, various beyond the Standard Model predictions (as discussed in Section 2.5.3), and experimental limits for all processes $t \rightarrow Xq$ where q is an up-type quark and X is any neutral boson.

Since the publication of Figure 2.14 the ATLAS experiment has published a result in the production mode of the $t \rightarrow q\gamma$ vertex using 81 fb^{-1} of data (LHC data runs between 2015-2017). Upper limits have been set on $t \rightarrow u\gamma$ left-handed (right-handed) branching ratio of 2.8×10^{-5} (6.1×10^{-5}) and upper limits on $t \rightarrow c\gamma$

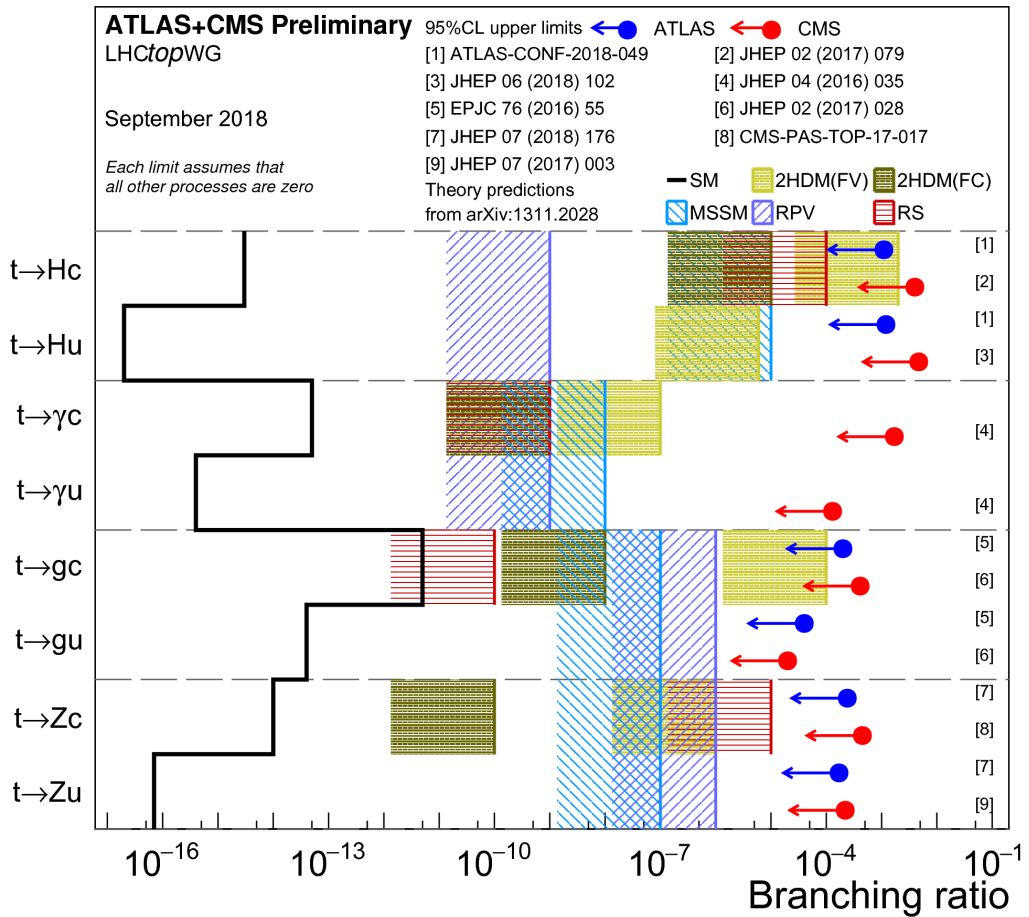


FIGURE 2.14. Flavor-changing neutral current theoretical branching ratios and experimental limits (both ATLAS and CMS) updated through 2018.

left-handed (right-handed) branching ratio of 22×10^{-5} (18×10^{-5}) [31]. Production mode searches offer better reach for $t \rightarrow u\gamma$ over $t \rightarrow c\gamma$ due to the higher prevalence of up quarks in the parton distribution function of the colliding protons.

This dissertation presents a complementary search for the process $t \rightarrow q\gamma$ to the ATLAS single top production search in the decay channel using top quark pair events. The process $t\bar{t} \rightarrow bWq\gamma \rightarrow bl\nu q\gamma$ will be searched for using the ATLAS detector. This final state ($bl\nu q\gamma$) is a straightforward channel in that it has one of each type of object that can be reconstructed with ATLAS. There are 2 jets from the quarks but one is a b-jet that has qualities that can distinguish it from a normal

quark jet which will be discussed in Section 4.2.3.1. In addition to the jets the final state also has a charged lepton (an electron or muon), a photon, and a neutrino. The reconstruction of these objects is discussed in Chapter IV. The FCNC process is a unique process where a top quark decays directly into an up-type quark and a photon. The jet and photon we measure are required to be reconstructed into a top quark by measuring the invariant mass requirement which gives an excellent handle for separating signal from background.

CHAPTER III

THE LARGE HADRON COLLIDER AND THE ATLAS DETECTOR

This chapter details the experimental details of the collider complex at the LHC and specifically the ATLAS detector used to produce, collect, and measure various particle properties. The subsystems of the ATLAS detector are described in detail.

3.1. The Large Hadron Collider

The LHC is the world's largest and most energetic particle accelerator. As a hadron collider the LHC collides particles made up of quarks, typically proton-proton collisions. Protons, as opposed to electrons/positrons at a previous collider such as LEP, have much higher mass and have a significantly smaller amount of energy loss during acceleration due to synchrotron radiation (which scales as $\frac{1}{m^4}$). Due to this the LHC is able to reach a much higher center of mass energy using the same circular ring used by LEP. This higher energy comes at a cost though. Due to hadrons being made up of constituent partons (quarks and gluons) not all of which interact in any given collision the particles that don't take place in the hard interaction are left over and create a 'messier' environment in the detectors. Whereas in lepton colliders all of the energy that goes into the collision is present in the final state particles coming from the interaction point. The implication of this is that hadron colliders cannot know the momentum along the beam axis and only know the momentum in the transverse plane due to conservation of momentum.

The LHC is housed in a 27 km ring running beneath the Franco-Swiss border near Geneva, Switzerland and accelerates beams of protons (ions) to a center of mass energy of 13 TeV (5 TeV) using two counterpropagating circular beams around the

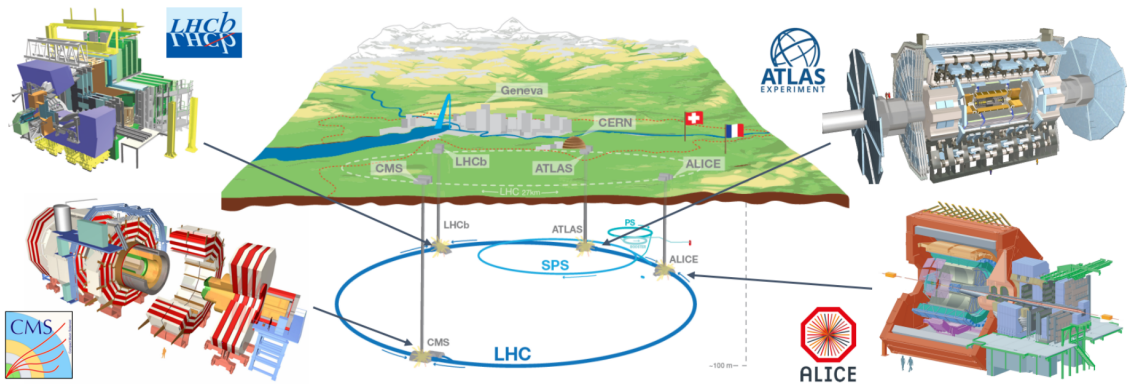


FIGURE 3.1. Map of LHC and the various detector experiments: ATLAS, CMS, LHCb, and ALICE located under the Franco-Swiss border near Geneva[35]

ring. The particles are then collided at one of the four primary interaction points, each of which house a dedicated detector as shown in Figure 3.1.

In addition to the LHC beam line the accelerator uses a series of smaller accelerators to increase the energy of the particles before being introduced into the LHC. This accelerator complex is detailed in Figure 3.2. The start of the accelerator chain, and source of LHC protons, is the Linear Accelerator 2 (LINAC 2, purple) where hydrogen gas is placed inside of an electric field which separates the protons and electrons. The remaining protons are passed through radiofrequency (RF) cavities and accelerated to 50 MeV using electric fields which oscillate at a frequency specific to the distance between any two RF cavities.

After leaving LINAC 2 the protons are injected into the Proton Synchrotron Booster (BOOSTER, light purple) and accelerated to 1.4 GeV before being passed to the Proton Synchrotron (PS, magenta) in two batches with a separation of 1.2 seconds. The PS accelerates the protons to 25 GeV to be injected into the Super Proton Synchrotron (SPS, blue) in a series of four batches separated by 3.6 seconds and are accelerated to 450 GeV. The SPS is the second largest accelerator in the complex. After being reaching the 450 GeV of the SPS the particles are split and

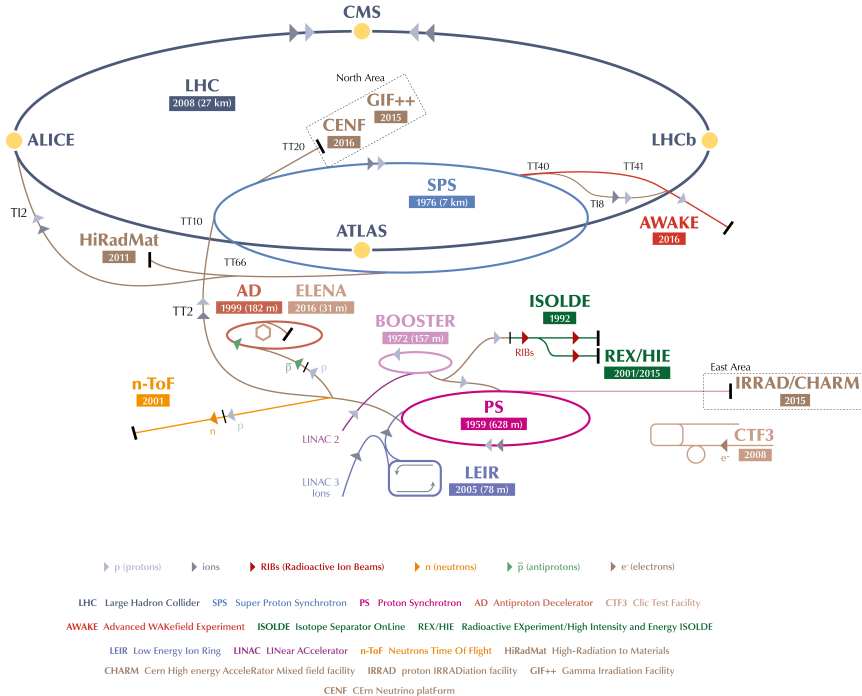


FIGURE 3.2. Schematic of the CERN accelerator complex.[32]

injected into the LHC in opposing directions where they are further accelerated to a collision energy of 6.5 TeV per beam leading to a center of mass energy of 13 TeV for the LHC during Run-2.

The first proton-proton collisions were produced in the LHC in 2008 at the injection energy of the SPS, $\sqrt{s} = 900$ GeV. During testing a faulty electrical connection caused a magnet quench, a sudden loss of superconductivity, to occur. This broke the nearby magnets and caused a delay in operations until late 2009 when LHC Run-1 began at a collision energy of $\sqrt{s} = 7$ TeV and later raised to $\sqrt{s} = 8$ TeV in 2012 to complete Run-1. Various upgrade and repairs on the LHC occurred throughout the long shutdown between 2012-2015 where the center of mass energy was increased to the LHC Run-2 energy of $\sqrt{s} = 13$ TeV.

3.1.1. LHC Magnets

The energies achieved in the collisions are only possible due to the LHC magnets that bend and focus the colliding particles. The LHC uses the most powerful magnet technology that can be produced on an industrial scale. There are 1232 superconducting dipole magnets each being 15m in length, weighing 35 tonnes, and producing uniform magnetic fields of up to 8.4 T. The niobium-titanium cables must be cooled to 1.9 K and operate with a current of 11,800 A. Of these 1232 magnets 1104 are used to bend the particles around the ring and the remaining 128 are used in the beam dump. To achieve the same center of mass energy using standard non-superconducting magnets the 27 km LHC would instead have to be upwards of 120 km long.

Since the bunches of particles are charged they will naturally diverge while traveling if not focused. To correct for this an additional 392 quadrupole magnets, 5-7m in length, are used to focus the beam. These quadrupoles are used in pairs: one which focuses in the horizontal plane and defocuses in the vertical plane and the other focuses in the vertical plane and defocuses in the horizontal plane. Together these magnets can keep the beam squeezed to a usable size. All of these magnets have two apertures, one for each of the counter-propagating beams.

3.1.2. Luminosity

The amount of data collected at collider experiments is determined not only by the center of mass energy of colliding particles but also the rate of events produced. This rate is called the luminosity and can be determined by the square of the number of particles in each bunch (since any one in one bunch can interact with any one in the other), the time between bunches, and the cross section of the bunch (or probability

of a collision).

$$\mathcal{L} = \frac{1}{\sigma} \frac{dN}{dt}$$

For any given proton-proton pair the luminosity can be expressed as:

$$\mathcal{L} = \frac{1}{4\pi\sigma_x\sigma_y}$$

and can be expanded for the whole beam with the inclusion of the number of protons per bunch (N_1 and N_2), the number of bunches (N_b), and the frequency at which the bunches overlap (f) to:

$$\mathcal{L} = \frac{N_1 N_2 N_b f}{4\pi\sigma_x\sigma_y}$$

which can be iterated over the running time of the LHC (the total time with beams of proper size and energy propagating through the LHC) giving the total delivered luminosity. This total integrated luminosity as a function of time during LHC Run-2 is shown in Figure 3.3. This luminosity value can be multiplied by the probability, or cross section, of any particular final state to obtain the number of times that final state is produced with a given luminosity.

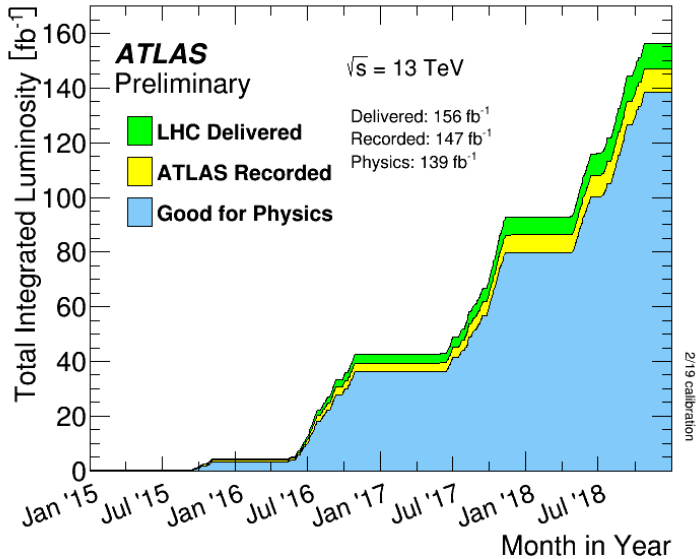


FIGURE 3.3. Total integrated luminosity as a function of time delivered by the LHC(green), recorded (yellow) and declared good for physics analysis (blue) by the ATLAS detector throughout Run 2 consisting entirely of 13 TeV pp collisions (figure from the ATLAS Collaboration).

3.1.3. Pileup

Increasing the luminosity is very beneficial for increasing the statistics needed when searching for rare events but it brings additional challenges as well. Most interactions at any given detector are not hard-scatter events that correspond to potentially interesting physics cases but are instead soft collisions which create noise in the various detector experiments. The LHC works hard to deliver as much data to the experiments as possible and delivers bunches of protons at a time. It is possible for multiple pairs of protons to undergo these soft inelastic collisions at a time. The average number of interactions per bunch crossing, or pileup $\langle \mu \rangle$, for Run-2 was 33.7, shown in Figure 3.4. The pileup must be accounted for when separating the tracks and energy deposited within a detector from an interesting hard-scatter event from the other soft collisions which occur at nearly the same time. The difficulty of

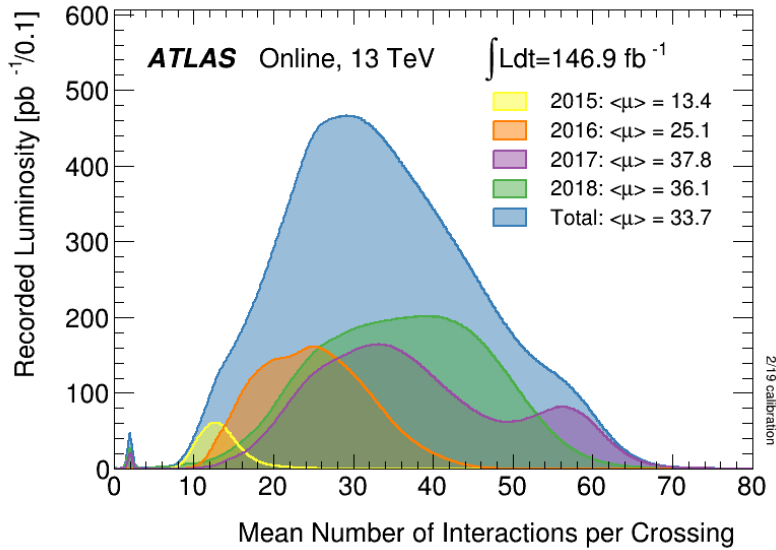


FIGURE 3.4. Luminosity-weighted distribution of the mean number of interactions per bunch crossing for the entirety of Run 2 shown by individual years, 2015 (yellow), 2016 (orange), 2017 (purple), 2018 (green), as well as an integrated total (blue) (figure from the ATLAS Collaboration).

separating out one event from another can be seen in Figure 3.5 where there are 28 reconstructed verticies. An extreme case of 65 reconstructed verticies is also shown in Figure 3.6. As the LHC will continue to operate in the future at higher and higher luminosities the amount of pileup that will need to be dealt with will continue to increase.

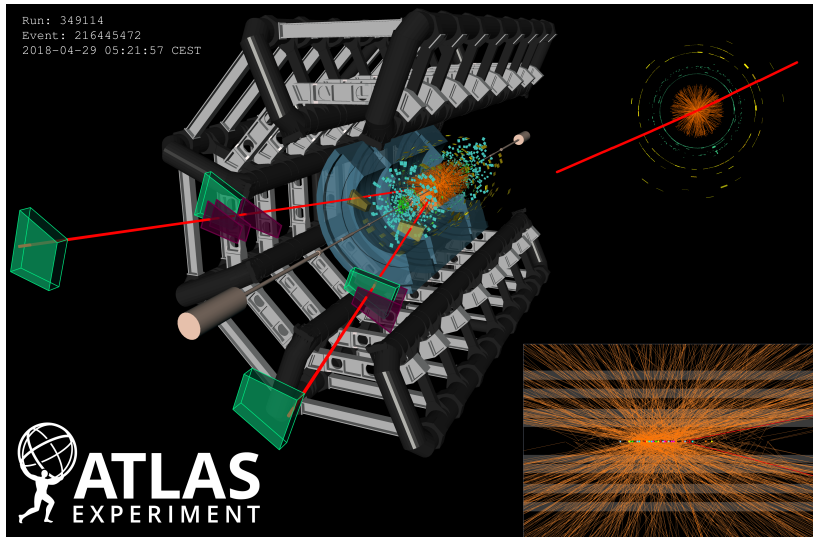


FIGURE 3.5. A candidate dimuon event ($Z \rightarrow \mu^+ \mu^-$) with 28 reconstructed verticies collected in 2018 with the ATLAS detector.

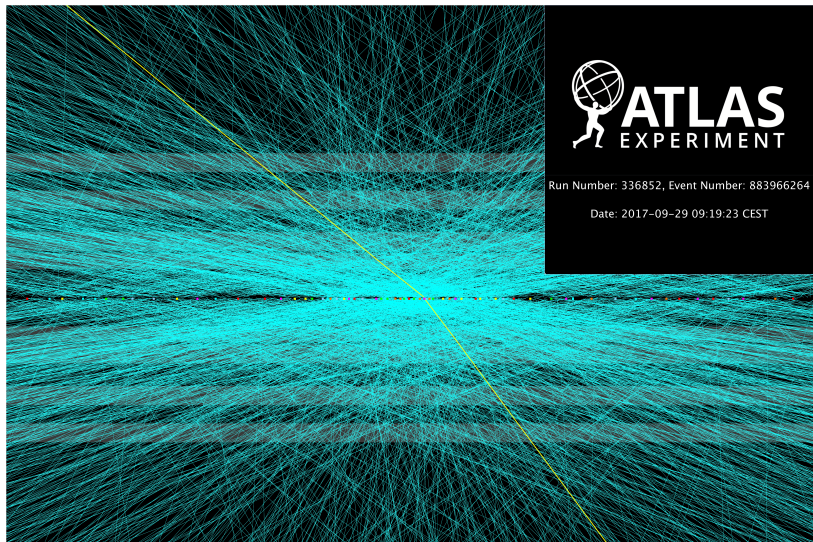


FIGURE 3.6. A candidate dimuon event ($Z \rightarrow \mu^+ \mu^-$) with 65 reconstructed verticies collected in 2017 with the ATLAS detector.

3.2. The ATLAS Detector

Section:ATLAS

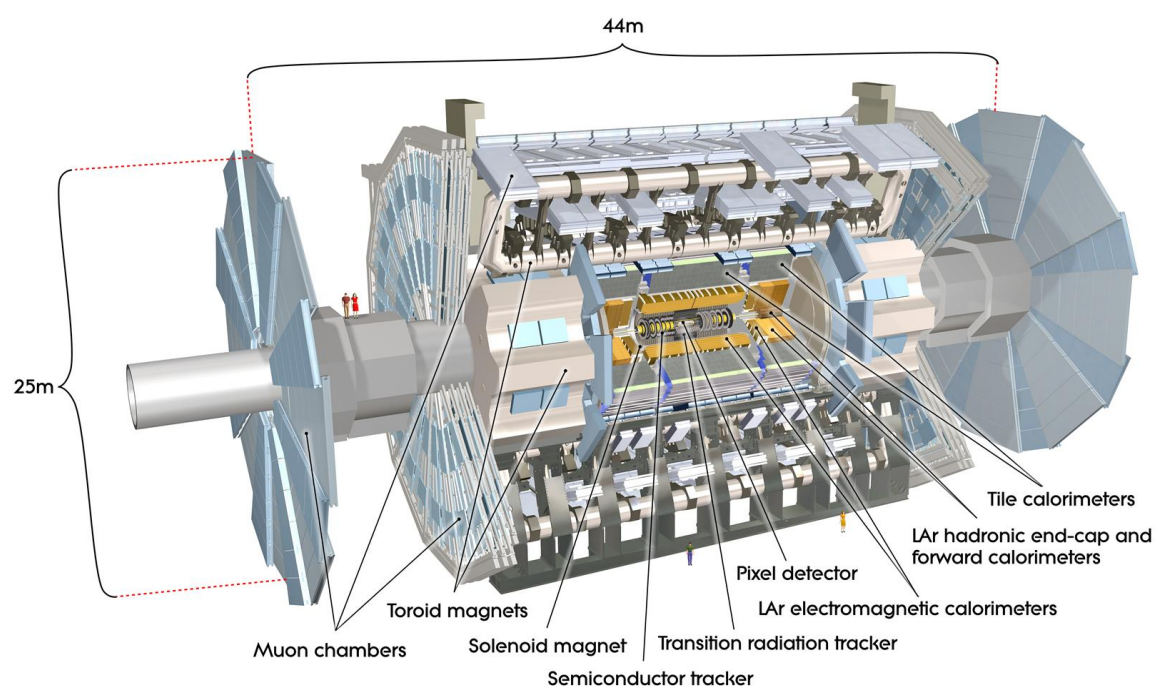


FIGURE 3.7. Schematic of the ATLAS detector.[33]

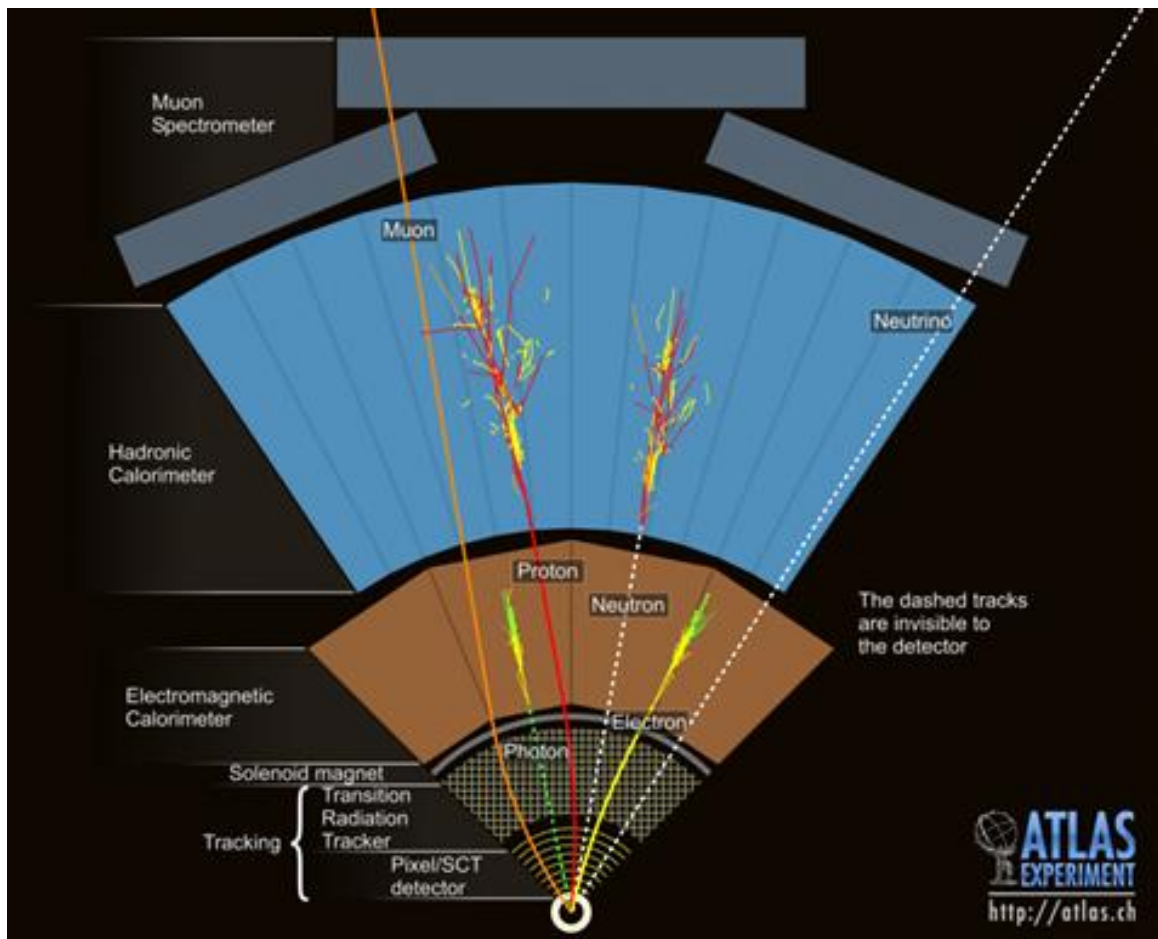


FIGURE 3.8. Cross section of a simulated ATLAS detector showing how various particles interact with ATLAS subsystems.[34]

3.2.1. Coordinate System

Coords

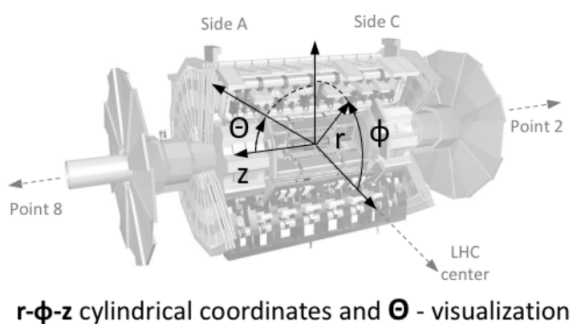
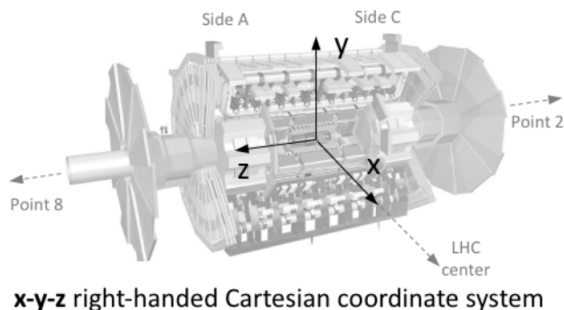


FIGURE 3.9. Coordinate system used in the ATLAS Collaboration.[35]

3.2.2. Magnet Setup

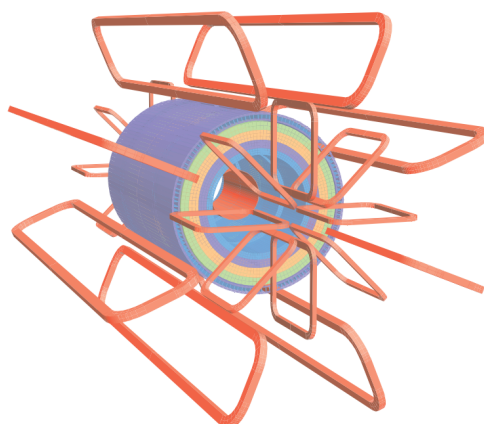


FIGURE 3.10. Schematic of the windings of the ATLAS magnet.[33]

3.2.3. Inner Detector

Inner

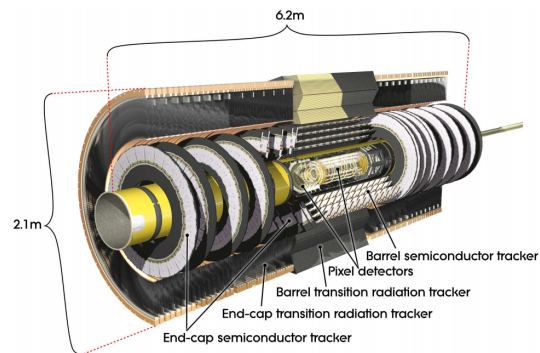


FIGURE 3.11. Schematic of the ATLAS inner detector.[33]

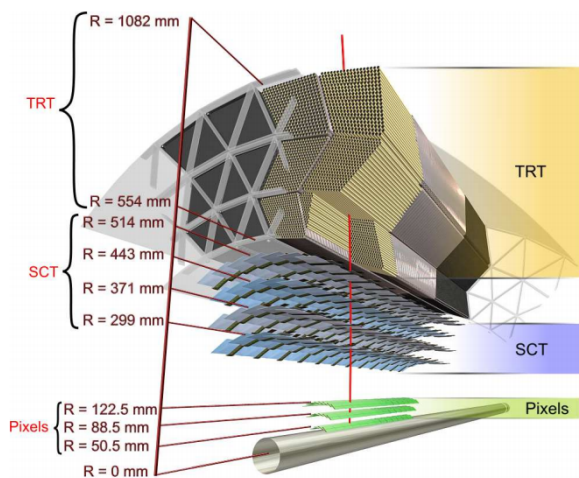


FIGURE 3.12. Blown up schematic of the ATLAS inner detector with more detail.[33]

3.2.4. Middle Layers, EMCAL, HCal

Middle chunks

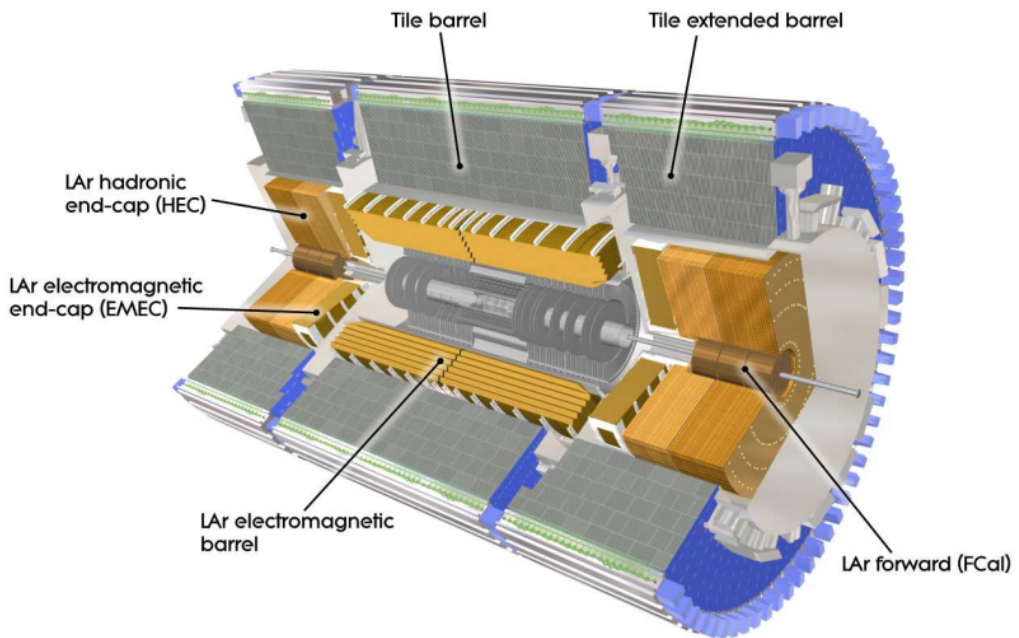


FIGURE 3.13. Schematic of the ATLAS hadronic and electromagnetic calorimeter systems.[33]

3.2.5. Muon Calorimeter

Muons have to get picked up I guess

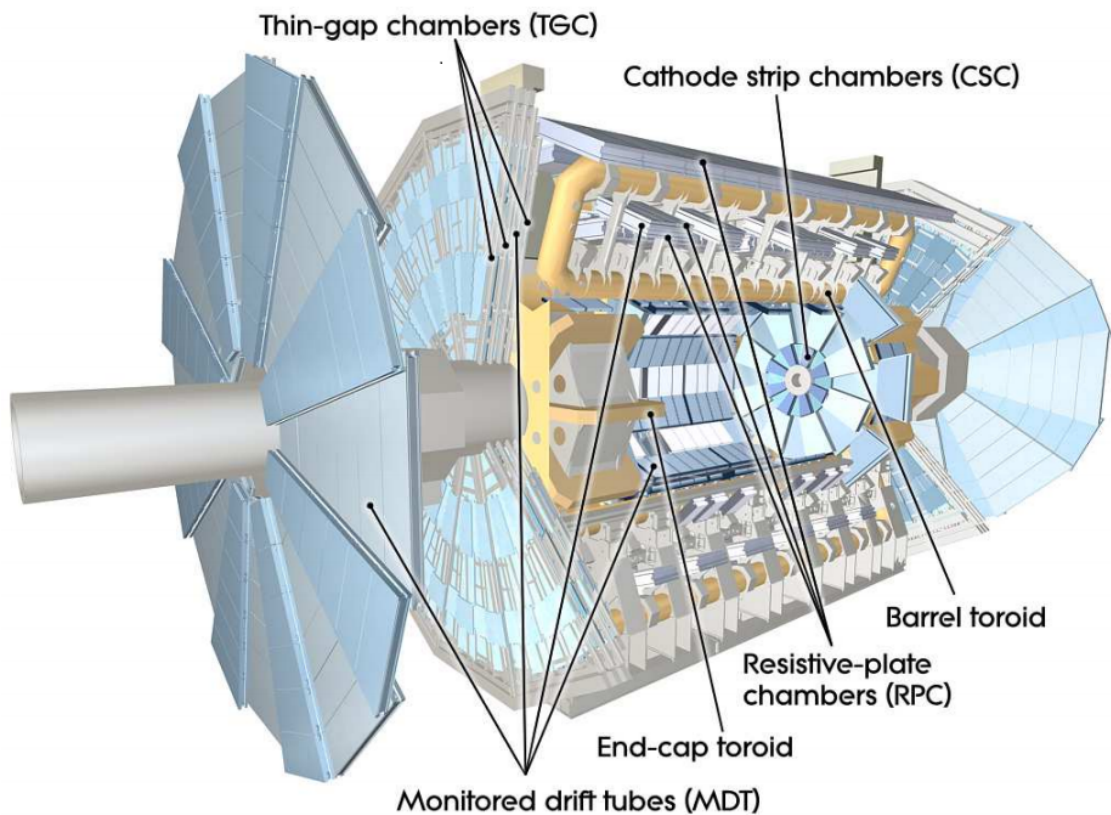


FIGURE 3.14. Schematic of the ATLAS muon detector.[33]

3.2.6. Trigger and Data Acquisition

All of these subsystems lead into actual data farm

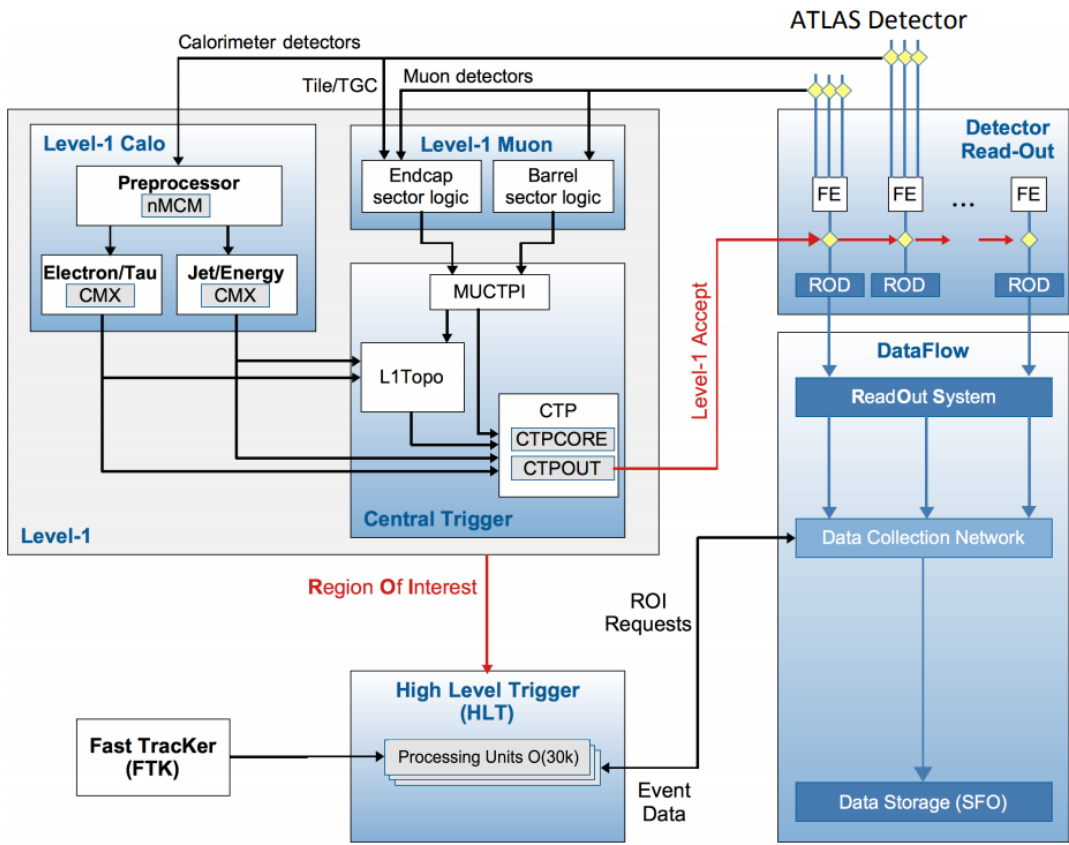


FIGURE 3.15. Flow diagram of the ATLAS trigger and data acquisition system used in Run 2.[36]

3.2.6.1. L1Calo

3.2.6.2. HLT

CHAPTER IV

SIMULATION

4.1. Simulation of pp collisions

4.1.1. MC Generators Used for LHC Physics

4.1.2. Detector Simulation

4.1.3. Showering in the Detector

4.2. Object Reconstruction

4.2.1. Electrons

4.2.2. Photons

4.2.3. Jets

4.2.3.1. B-Jets

4.2.4. Muons

4.2.5. Creation of FCNC Signal Events

4.2.5.1. MadGraph5 amc@NLO

Comparison of kinematics between standard ttbar events ATLAS Production of these events TopQ1 Slimming/Skimming

CHAPTER V

SEARCH STRATEGY

5.1. Major Backgrounds

5.2. Event Reconstruction

5.3. Data and Simulation Event PreSelection

5.4. Control and Validation Regions

5.5. Signal Region

5.6. Neural Network

5.6.1. Architecture and Studies

CHAPTER VI

RESULTS

6.1. Uncertainties

6.2. Statistical Treatment of Results

6.3. Limit on Branching Ratio $t \rightarrow q\gamma$

CHAPTER VII

COMPLEMENTARY SEARCHES AND OUTLOOK

7.1. Comparison with Complementary Searches

7.2. Future Directions

HL-LHC and Beyond Future prospectives at Linear Colliders? - <https://www.sciencedirect.com>

7.3. Conclusion

REFERENCES CITED

- [1] S. L. Glashow. Partial Symmetries of Weak Interactions. *Nucl. Phys.*, 22:579–588, 1961.
- [2] Peter W. Higgs. Broken Symmetries and the Masses of Gauge Bosons. *Phys. Rev. Lett.*, 13:508–509, 1964. [,160(1964)].
- [3] F. Englert and R. Brout. Broken Symmetry and the Mass of Gauge Vector Mesons. *Phys. Rev. Lett.*, 13:321–323, 1964. [,157(1964)].
- [4] Steven Weinberg. A Model of Leptons. *Phys. Rev. Lett.*, 19:1264–1266, 1967.
- [5] Abdus Salam. Weak and Electromagnetic Interactions. *Conf. Proc.*, C680519:367–377, 1968.
- [6] Georges Aad et al. Observation of a new particle in the search for the Standard Model Higgs boson with the ATLAS detector at the LHC. *Phys. Lett.*, B716:1–29, 2012.
- [7] Serguei Chatrchyan et al. Observation of a new boson at a mass of 125 GeV with the CMS experiment at the LHC. *Phys. Lett.*, B716:30–61, 2012.
- [8] F. Abe et al. Observation of top quark production in $\bar{p}p$ collisions. *Phys. Rev. Lett.*, 74:2626–2631, 1995.
- [9] The ATLAS collaboration. Measurement of the top quark mass in the $t\bar{t} \rightarrow$ lepton+jets channel from $\sqrt{s}=8$ TeV ATLAS data. 2017.
- [10] M. Tanabashi et al. Review of Particle Physics. *Phys. Rev.*, D98(3):030001, 2018.
- [11] J. J. Cao, G. Eilam, M. Frank, K. Hikasa, G. L. Liu, I. Turan, and J. M. Yang. SUSY-induced FCNC top-quark processes at the large hadron collider. *Phys. Rev.*, D75:075021, 2007.
- [12] Junjie Cao, Zhaoxia Heng, Lei Wu, and Jin Min Yang. R-parity violating effects in top quark FCNC productions at LHC. *Phys. Rev.*, D79:054003, 2009.
- [13] G. Eilam, J. L. Hewett, and A. Soni. Rare decays of the top quark in the standard and two Higgs doublet models. *Phys. Rev.*, D44:1473–1484, 1991. [Erratum: Phys. Rev.D59,039901(1999)].
- [14] Yuval Grossman. Introduction to flavor physics. In *Flavianet School on Flavour Physics Karlsruhe, Germany, September 7-18, 2009*, pages 111–144, 2014. [,73(2014)].

- [15] Nicola Cabibbo. Unitary Symmetry and Leptonic Decays. *Phys. Rev. Lett.*, 10:531–533, 1963. [,648(1963)].
- [16] Makoto Kobayashi and Toshihide Maskawa. CP Violation in the Renormalizable Theory of Weak Interaction. *Prog. Theor. Phys.*, 49:652–657, 1973.
- [17] Lincoln Wolfenstein. Parametrization of the Kobayashi-Maskawa Matrix. *Phys. Rev. Lett.*, 51:1945, 1983.
- [18] S. L. Glashow, J. Iliopoulos, and L. Maiani. Weak Interactions with Lepton-Hadron Symmetry. *Phys. Rev.*, D2:1285–1292, 1970.
- [19] S. W. Herb et al. Observation of a Dimuon Resonance at 9.5-GeV in 400-GeV Proton-Nucleus Collisions. *Phys. Rev. Lett.*, 39:252–255, 1977.
- [20] S. Abachi et al. Search for high mass top quark production in $p\bar{p}$ collisions at $\sqrt{s} = 1.8$ TeV. *Phys. Rev. Lett.*, 74:2422–2426, 1995.
- [21] Markus Cristinziani and Martijn Mulders. Top-quark physics at the Large Hadron Collider. *J. Phys.*, G44(6):063001, 2017.
- [22] J. A. Aguilar-Saavedra. Top flavor-changing neutral interactions: Theoretical expectations and experimental detection. *Acta Phys. Polon.*, B35:2695–2710, 2004.
- [23] David Atwood, Laura Reina, and Amarjit Soni. Phenomenology of two Higgs doublet models with flavor changing neutral currents. *Phys. Rev.*, D55:3156–3176, 1997.
- [24] J. A. Aguilar-Saavedra and B. M. Nobre. Rare top decays $t \rightarrow l c \gamma$, $t \rightarrow l c g$ and CKM unitarity. *Phys. Lett.*, B553:251–260, 2003.
- [25] J. A. Aguilar-Saavedra. Effects of mixing with quark singlets. *Phys. Rev.*, D67:035003, 2003. [Erratum: Phys. Rev.D69,099901(2004)].
- [26] Jin Min Yang, Bing-Lin Young, and X. Zhang. Flavor changing top quark decays in r parity violating SUSY. *Phys. Rev.*, D58:055001, 1998.
- [27] Kaustubh Agashe, Gilad Perez, and Amarjit Soni. Collider Signals of Top Quark Flavor Violation from a Warped Extra Dimension. *Phys. Rev.*, D75:015002, 2007.
- [28] Mark Trodden. Electroweak baryogenesis. *Rev. Mod. Phys.*, 71:1463–1500, 1999.
- [29] G. C. Branco, P. M. Ferreira, L. Lavoura, M. N. Rebelo, Marc Sher, and Joao P. Silva. Theory and phenomenology of two-Higgs-doublet models. *Phys. Rept.*, 516:1–102, 2012.

- [30] Andreas Crivellin and Ulrich Nierste. Chirally enhanced corrections to FCNC processes in the generic MSSM. *Phys. Rev.*, D81:095007, 2010.
- [31] Georges Aad et al. Search for flavour-changing neutral currents in processes with one top quark and a photon using 81 fb^{-1} of pp collisions at $\sqrt{s} = 13 \text{ TeV}$ with the ATLAS experiment. 2019.
- [32] Esma Mobs. The CERN accelerator complex. Complex des accélérateurs du CERN. Jul 2016. General Photo.
- [33] The ATLAS Experiment at the CERN Large Hadron Collider. *J. Instrum.*, 3:S08003. 437 p, 2008.
- [34] Joao Pequenao. Event Cross Section in a computer generated image of the ATLAS detector. Mar 2008.
- [35] Fabian Kuger. Signal formation processes in micromegas detectors and quality control for large size detector construction for the atlas new small wheel. 08 2017.
- [36] Moritz Backes. The ATLAS Trigger System: Ready for Run-2. *PoS*, LeptonPhoton2015:045, 2016.